Smart Structures and Systems, *Vol. 27, No. 2 (2021) 173-191*
DOI: https://doi.org/10.12989/sss.2021.27.2.173

Structural identification of the dynamic behavior of floor diaphragms in existing buildings

Daniele Sivori*, Marco Lepidi [a] and Serena Cattari [b]

Department of Civil, Chemical and Environmental Engineering (DICCA), University of Genoa, Via Montallegro 1, Genoa 16145, Italy

(*Received August 25, 2020, Revised October 26, 2020, Accepted November 25, 2020*)

Abstract. The deformability of floor diaphragms plays a primary role in the structural behavior of existing buildings. Nonetheless, few structural identification procedures are available to investigate this matter from in-situ experimental measurements. Ambient vibration tests can be very useful to the purpose, allowing to assess the importance of the floor deformability in operational modal analyses through model-driven approaches. This information is particularly valuable for unreinforced masonry buildings, often characterized by deformable diaphragms whose effective stiffness is commonly unknown and hard to be evaluated. Based on these motivations, in this paper, a discrete linear model of deformable diaphragm is formulated in a novel fashion. The modal properties governing the free undamped dynamics are analytically determined through a fully general perturbation technique (direct problem). Therefore, a model-based structural identification procedure is proposed to analytically assess the inertial and elastic properties of the deformable diaphragm (inverse problem), assuming the outcomes of experimental modal analyses as known input. Consistently with the perturbation approach, explicit formulas are determined for low-order minimal models and higher-order model updating, accounting for mass and inertial eccentricities. Among the other identifiable mechanical parameters, the focus is put on the first and second-order identification of the in-plane shear stiffness of the diaphragm. The theoretical developments are successfully verified on pseudo-experimental and experimental bases, by applying the identification procedure to (i) the computational model of a prototypical steel frame structure, (ii) the large scale laboratory model of a two-story composite structure with mass eccentricities, (iii) a permanently monitored masonry building recently struck by the 2016-2017 Central Italy earthquake sequence.

Keywords: diaphragm deformability; perturbation methods; structural identification; model updating; ambient vibration tests; existing buildings

1. Introduction

The structural models – ranging from synthetic parametric formulations to high-fidelity computational descriptions – constitute fundamental tools in modern engineering to assess the safety of structures in operating and seismic conditions, both through rapid procedures (Michel *et al*. 2012, Iervolino *et al*. 2014, Spina *et al*. 2019) and refined numerical analyses (see for example Lupoi *et al*. 2004, Derkevorkian *et al*. 2014).

Within the field of existing buildings, the definition of reliable dynamic models requires the correct interpretation of the inertial, dissipative and elastic properties that, altogether, may determine the global and local structural response, influenced by a variety of materials and structural details. Furthermore, a long-dating history of past structural modifications and/or retrofitting interventions may play a non-negligible role in worsening or improving the present performance of aged buildings. The knowledge phase – whose process is coded by several national and international regulations (including EN19983 2005, ASCE 41-13 2014, NTC 2018, NZSEE 2017) – is currently an interesting matter of research, mainly aimed at the conceptual development and systematic implementation of standard procedures (Jalayer *et al*. 2010, Kosič *et al*. 2014, Bracchi *et al*. 2015). The preliminary investigation phase is targeted at reducing the unavoidable uncertainties (Haddad *et al*. 2019) – regarding the geometry, the structural typology, the mechanical properties of the materials, the nature, quality and effectiveness of the elements and constraints – and, eventually, at guiding the assumption of the modeling hypotheses that most accurately describe the actual structural behavior.

Among the others, a common modeling hypothesis regards the in-plane behavior of the floor diaphragms (Kunnath *et al*. 1991). Although some structural typologies, such as reinforced concrete or steel buildings, can be reasonably associated with the hypothesis of perfectly rigid diaphragms (Greco *et al*. 2020), this assumption is much more problematic for existing masonry buildings, which constitute the principal application field of the present article. The difficulties arise, on the one hand, from the great variety of diaphragm typologies (timber floors, vaults, steel beams and hollow clay blocks, concrete slabs, etc.) and, on the other hand, from the role played by the connection with the vertical walls in the dynamic response

*Corresponding author, Ph.D. Student,
E-mail: daniele.sivori@dicca.unige.it
[a] Associate Professor, E-mail: marco.lepidi@unige.it
[b] Associate Professor, E-mail: serena.cattari@unige.it

ISSN: 1738-1584 (Print), 1738-1991 (Online)

of the structure. Within this framework, the likely occurrence of moderate to severe seismic damages may add a remarkable source of structural uncertainties, in post-earthquake scenarios.

In the field of structural models for seismic analysis, the in-plane shear stiffness assigned to the floor diaphragms can significantly influence the safety assessment evaluations, especially for masonry buildings. Regarding seismic safety, the Italian National Building Code NTC 2018 explicitly states that a global three-dimensional structural analysis is suitable only if the diaphragm stiffness suffices to guarantee an efficient redistribution of the horizontal actions among the vertical walls in the linear and nonlinear regime. Otherwise, additional evaluations regarding possible local mechanisms are required. Furthermore, in the safety evaluations based on nonlinear static analyses – the most common choice for existing masonry buildings – the assessment is considerably sensitive to the variation of the diaphragm stiffness (Nakamura *et al*. 2017), with further potential repercussions on the definition of the damage limit states on the pushover curve (Cattari *et al*. 2015, Marino *et al*. 2019).

In this regard, the recent observations of the seismic damage caused by the 2009 L'Aquila earthquake – made available by the Italian Department of Civil Protection through the Da.D.O platform (Dolce *et al*. 2019) – pointed out the importance of the in-plane deformability of floor diaphragms in the seismic response of masonry buildings (Del Gaudio *et al*. 2019, Rosti *et al*. 2020). These research studies highlight the greater seismic vulnerability of buildings characterized by vaults (aggravated by out-of-plane actions, often in absence of retaining steel tie-rods) and, in general, deformable floors. This finding is also indirectly confirmed by the seismic vulnerability reduction factors proposed in presence of quasi-rigid floors coupled to edge beams (Lagomarsino and Giovinazzi 2006). On the contrary, it is well established that the in-plane stiffness of floor diaphragms positively influences the global dynamic behavior of the structure, ensuring the lateral load redistribution and reducing the level of potential damage. Thus, deepening the knowledge on this topic is a matter of theoretical and applied interest, especially to the purpose of formulating or updating consistent analytical, computational and experimental models.

To this end, the support of structural diagnostic investigations is fundamental. If several in-situ tests are available to investigate the material properties (for the masonry see Kržan *et al*. 2015, Boschi *et al*. 2019), much less are the experimental techniques proposed to evaluate the stiffness of floor diaphragms. Some solutions have been proposed to investigate the stiffness of timber floors and the effectiveness of their connections to the vertical walls (Giongo *et al*. 2015, Dizhur *et al*. 2020, Rizzi *et al*. 2020). For other floor typologies, such as vaults, these studies are usually carried out in a laboratory environment (Rossi *et al*. 2016, 2017) or through numerical simulations (Cattari *et al*. 2008). Within this context, the use of ambient vibration measurements to deduct global information on the structure seems increasingly promising. The cost reduction of the experimental instruments and the continuous development of smart and powerful algorithms of data processing, accompanied also by the growing competencies of the technicians, makes nowadays economically and operationally feasible the rapid diffusion in the current engineering practice of evaluation procedures previously confined to strategic (Mori and Spina 2015) or monumental structures (Karatzetzou *et al*. 2015, Gattulli *et al*. 2016). In this sense, the number of existing buildings for which instrumental data and experimental modal information are available is rapidly growing, thanks also to monitoring projects at the national scale (Dolce *et al*. 2017, Astorga *et al*. 2020). It is not utopian the outlook that, in the next future, the availability of such information will be extended to cover the entire stock of buildings exposed to seismic risk.

Based on the above motivations, the paper postulates the initial availability of synthetic spectral data resulting from modal experimental analyses (first-level modal identification problem), suited to identify and discriminate rigid-diaphragm modes from deformable ones (Sivori *et al*. 2020). Starting from this solid background of information, the main objective of the paper is to state and solve the inverse structural problem of identifying the diaphragm in-plane shear stiffness of existing buildings (second-level parametric or structural identification problem). The model-driven nature of the structural problem makes it naturally more complex to be inverted, either analytically or numerically. Furthermore, the formulation of the direct problem (model dimension, mechanical assumptions), as well as the methodological tools (exact, approximate) employed to solve the governing equations, may compromise the existence and uniqueness of the inverse problem solution.

A mature and well-established field of research exists – the model updating of high-fidelity finite element models – which may serve the purpose. Most of the updating techniques attempt to solve an optimization problem, seeking for the value of one or more structural parameters which minimizes the residual between the model predictions and the experimental results (Zárate and Caicedo 2008).

The most recent and successful developments rely on the sensitivity method (Jaishi and Ren 2005, Reynders *et al*. 2010, Mottershead *et al*. 2011), which, based on the linearization of the residual function, exploits an iterative scheme to update the most sensitive parameters. In general, the reliability of these techniques depends on several factors – the choice of an appropriate objective function, the feasibility of the numerical model, the efficiency of the optimization algorithm – but, primarily, on the well-posedness of the inverse problem. That is to say, since the number of variables is usually larger than the equations available, more than one optimum solution may exist.

In this paper, the same issue is tackled from a novel perspective. Among the other possibilities, a low-dimension linear model of the diaphragm is formulated to describe the free undamped dynamics of the entire floor or one (or more) of its spans (Section 2). An extra dynamically-active degree-of-freedom is purposely introduced to account for the shear deformability of the diaphragm. The model mass

and stiffness matrices are built analytically (Section 2.1) and the direct eigenproblem governing the modal properties is stated and solved (Section 2.2). The eigensolution is obtained in a suited analytic – although asymptotically approximate – fashion. In this respect, the multiparameter perturbation technique employed can be applied also to larger dimension models, described by a generic number of mechanical parameters. The low-order approximate solution can be properly inverted (Section 2.3) to identify the unknown stiffness parameters (Section 2.3.1). Among the others, the parameter governing the in-plane shear stiffness of the diaphragm is derived analytically, as an explicit function only of the experimental frequencies of the rigid and deformability modes. This guarantees the existence and uniqueness of a solution, within the class of mass and stiffness properties described by the low-dimension analytical model. Since the solution reliability, however, depends on how faithfully the analytical model can synthetically describe the real structure, the accuracy of the approximation and its range of validity are discussed. In this respect, the proposal is verified through pseudo-experimental data, numerically generated from the finite element model of a simple frame structure (Section 3). Finally, the effectiveness of the procedure is tested experimentally (Section 4), employing firstly experimental data from laboratory tests on scaled models (Section 4.1) and, lastly, vibration recordings from the full-scale monitoring of an existing masonry building (Section 4.2).

2. Dynamic model of deformable diaphragm

In the mechanical formulation of analytical or computational models for building engineering, the generic building floor can be typically and efficiently described as a planar, horizontal and massive diaphragm connecting all the geometric vertices of the floor plan. From the structural viewpoint, the stiffness of the diaphragm in its own plane may strongly depend on many different technical aspects, including – among the others – the construction typology, the building materials and the efficiency of the connections among different resistant members (as discussed in NZSEE 2017 for timber floors and, more in general, in Solarino *et al*. 2019). Within this multifaceted scenario, introducing a priori the assumption of infinitely in-plane rigid diaphragms to reduce the computational effort of structural analyses can turn out to be an inaccurate simplification or, at least, an avoidable loss of generality.

To properly balance the opposite requirements of model synthesis and representativeness, the novel idea is to preserve a minimal description of the diaphragm deformability, without significantly increasing the complexity of the computational analyses. To this purpose, a single stationary displacement mode, kinematically compatible with a small deformation field, is admitted and superimposed to the rigid displacements of the diaphragm. To specify, the diaphragm is certainly allowed to move rigidly, as well as to develop small deformations according to an assigned geometric transformation of its initial configuration (referred to as *deformability mode* and assumed to preserve planarity). The amplitude of the deformability mode plays the role of an extra degree-of-freedom of the dynamic model, characterized by its own mass and stiffness. Even if – in principle – the deformability mode could be fixed arbitrarily, energetic criteria could be adopted to select – in practice – the transformation of the diaphragm configuration associated with the lowest possible elastic energy. In may be worth noting that, if necessary, more than one deformability mode could be taken into account.

For the purposes of the present work, a rectangular diaphragm with length $2A$, width $2B$ is considered (Fig. 1(a)). The translational mass M and rotational inertia J are univocally determined by assuming uniform mass density for unit area. The planar rigid motion of the diaphragm is fully described by the in-plane time-dependent displacements U and V and rotation θ of the configurational node (*central node* G), located at its centroid (Fig. 1(b)). Among the other possibilities and on the base of energetic considerations, the deformability mode selected to account for the diaphragm deformation is the *shear mode* that transforms a rectangle into a parallelogram by stretching the rectangle diagonals (the transformation represented in Fig. 1(c)). The angular defect of verticality assumed by the left and right sides of the rectangle, which can also be straightforwardly related to the loss of orthogonality between the rectangle sides, is chosen as modal amplitude. In analogy with the classic nomenclature of solid mechanics, it can be also conventionally referred to as *shear strain* Γ.

In order to accurately represent the mechanical behavior of buildings, the diaphragm vertices must be considered configurational nodes (*peripheral nodes*) of the mechanical model. The masses and stiffnesses of these nodes may

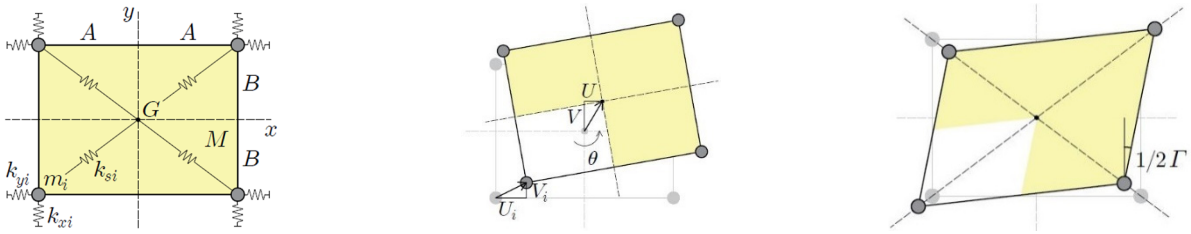

(a) Reference configuration (b) Rigid-body motions (c) Shear deformability

Fig. 1 Deformable mass-spring model of the rectangular diaphragm: (a) reference configuration with geometric, inertial and elastic properties; (b) dynamic configuration generated by the rigid-body motions; (c) dynamic configuration generated by the *shear deformability mode*

depend on a variety of technical aspects, starting from their connection degree with the structural members of the three-dimensional resistant structure of the building. To the purposes of the present work, it may be sufficient to consider four massive rotation-free peripheral nodes, located at the vertices of the rectangular diaphragm (Fig. 1(a)) and provided with point mass m_i and linear elastic stiffnesses k_{xi} and k_{yi} along the rectangle sides (i = 1, …, 4). The in-plane motion of the i-th node is fully described by the in-plane time-dependent displacements U_i and V_i.

According to the mechanical hypotheses, the forced dynamics of the deformable diaphragm is governed by a discrete elastic model, which can be considered linear as long as the displacement and modal amplitude are assumed sufficiently small. The model response can more conveniently be analyzed by introducing nondimensional independent and dependent variables

$$\tau = \Omega_r t, \quad u = \frac{U}{L_r}, \quad v = \frac{V}{L_r}, \quad u_i = \frac{U_i}{L_r}, \quad v_i = \frac{V_i}{L_r} \tag{1}$$

where Ω_r and L_r are known frequency and length – for example, the first (circular) natural frequency of the rectangular diaphragm model and the length of its diagonal – suited to serve as references for the time and space nondimensionalization, respectively. A minimal set $\boldsymbol{\mu}$ of nondimensional parameters sufficient to completely describe the structural properties of the dynamic model is

$$\begin{aligned} &\beta = \frac{B}{A}, && \varrho_i^2 = \frac{m_i}{M}, && \chi^2 = \frac{J}{ML_r^2}, \\ &\kappa_{xi} = \frac{k_{xi}}{M\Omega_r^2}, && \kappa_{yi} = \frac{k_{yi}}{M\Omega_r^2}, && \kappa_s = \frac{k_s}{M\Omega_r^2} \end{aligned} \tag{2}$$

where β is the *aspect ratio* of the rectangular diaphragm, ϱ_i^2 is the mass ratios between the mass attributed to the i-th peripheral node and the diaphragm mass, χ^2 is the rotational-to-translational mass of the diaphragm. Finally, the parameter κ_s synthetically accounts for the modal stiffness of the deformable diaphragm and can be interpreted as the equivalent nondimensional axial stiffness of a pair of identical diagonal bracings, elastically retaining the deformability mode.

2.1 Equations of motion

The linear equations of motions governing the forced dynamics of the mechanical model can be obtained by applying the Hamilton Principle for non-dissipative discrete systems excited by conservative external forces. Collecting the planar degrees-of-freedom of all the configuration nodes in the twelve-by-one column vector $\mathbf{u} = (u_1, v_1, u_2, v_2, u_3, v_3, u_4, v_4, u, v, \theta, \Gamma)$, the Hamilton action $\mathcal{H}$ can be expressed as

$$\mathcal{H} = \mathcal{K} - \mathcal{V} = \frac{1}{2}\dot{\mathbf{u}}^\top \mathbf{M}\dot{\mathbf{u}} - \left(\frac{1}{2}\mathbf{u}^\top \mathbf{K}\mathbf{u} - \mathbf{u}^\top \mathbf{b}\right) \tag{3}$$

where $\mathcal{K}$ and $\mathcal{V}$ are the nondimensional kinetic and potential energies, respectively, depending on the symmetric twelve-by-twelve mass and stiffness matrices $\mathbf{M}$ and $\mathbf{K}$, which are reported in Appendix A.1. The twelve-by-one vector $\mathbf{b}$ collects column-wise the external forces acting on all the degrees-of-freedom.

Introducing a suited partition $\mathbf{u} = (\mathbf{q}, \mathbf{s})$ to distinguish the column subvector $\mathbf{q}$ collecting the free degrees-of-freedom (or Lagrangian coordinates) from the column subvector $\mathbf{s}$ collecting the slave degrees-of-freedom, the kinetic and potential energies can be expressed in partitioned form

$$\begin{aligned} \mathcal{K} &= \frac{1}{2}\begin{pmatrix}\dot{\mathbf{q}}\\ \dot{\mathbf{s}}\end{pmatrix}^\top \begin{bmatrix}\mathbf{M}_{qq} & \mathbf{M}_{qs}\\ \mathbf{M}_{sq} & \mathbf{M}_{ss}\end{bmatrix}\begin{pmatrix}\dot{\mathbf{q}}\\ \dot{\mathbf{s}}\end{pmatrix} \\ \mathcal{V} &= \frac{1}{2}\begin{pmatrix}\mathbf{q}\\ \mathbf{s}\end{pmatrix}^\top \begin{bmatrix}\mathbf{K}_{qq} & \mathbf{K}_{qs}\\ \mathbf{K}_{sq} & \mathbf{K}_{ss}\end{bmatrix}\begin{pmatrix}\mathbf{q}\\ \mathbf{s}\end{pmatrix} - \begin{pmatrix}\mathbf{q}\\ \mathbf{s}\end{pmatrix}^\top \begin{pmatrix}\mathbf{b}_q\\ \mathbf{b}_s\end{pmatrix} \end{aligned} \tag{4}$$

where the relations $\mathbf{M}_{sq}^\top = \mathbf{M}_{qs}$ and $\mathbf{K}_{sq}^\top = \mathbf{K}_{qs}$ hold between the submatrices, for the sake of symmetry.

If the internal constraints between the slave and free degrees-of-freedom are linear holonomic, bilateral and time-independent, the constraining relations can conveniently be expressed in the matrix form $\mathbf{s} = \mathbf{V}\mathbf{q}$, where $\mathbf{V}$ is a rectangular constraint matrix. Consequently, the kinetic and potential energies of the constrained system can be expressed in the reduced space of the Lagrangian coordinates

$$\mathcal{K} = \frac{1}{2}\dot{\mathbf{q}}^\top\left(\mathbf{M}_{qq} + \mathbf{M}_{qs}\mathbf{V} + \mathbf{V}^\top\mathbf{M}_{sq} + \mathbf{V}^\top\mathbf{M}_{ss}\mathbf{V}\right)\dot{\mathbf{q}} \tag{5}$$

$$\begin{aligned} \mathcal{V} = \frac{1}{2}\mathbf{q}^\top&\left(\mathbf{K}_{qq} + \mathbf{K}_{qs}\mathbf{V} + \mathbf{V}^\top\mathbf{K}_{sq} + \mathbf{V}^\top\mathbf{K}_{ss}\mathbf{V}\right)\mathbf{q} \\ &-\mathbf{q}^\top\left(\mathbf{b}_q + \mathbf{V}^\top\mathbf{b}_s\right) \end{aligned} \tag{6}$$

and finally, imposing the action stationarity, the nondimensional equations of motion read

$$\mathbf{M}_q\ddot{\mathbf{q}} + \mathbf{K}_q\mathbf{q} = \mathbf{f} \tag{7}$$

where $\mathbf{M}_q = \mathbf{M}_{qq} + \mathbf{M}_{qs}\mathbf{V} + \mathbf{V}^\top\mathbf{M}_{sq} + \mathbf{V}^\top\mathbf{M}_{ss}\mathbf{V}$ and $\mathbf{K}_q = \mathbf{K}_{qq} + \mathbf{K}_{qs}\mathbf{V} + \mathbf{V}^\top\mathbf{K}_{sq} + \mathbf{V}^\top\mathbf{K}_{ss}\mathbf{V}$ are the symmetric mass and stiffness matrices of the constrained system, while $\mathbf{f} = \mathbf{b}_q + \mathbf{V}^\top\mathbf{b}_s$ is the column vector of the forces acting on the Lagrangian coordinates.

According to the motivations of the present work, two physical alternatives – following from the different definitions of the constraint matrix $\mathbf{V}$ – are analyzed and discussed in the following. The first possibility consists in assuming the diaphragm extremely stiff in its own plane. Consequently, internal constraints of (ideally) perfect rigidity between the central node and the peripheral nodes can be imposed on the mechanical model (the corresponding twelve-by-three constraint matrix $\mathbf{V}_r$ is reported in Appendix A.1). The resulting constrained model, characterized by the three-by-one vector $\mathbf{q}_r = (u, v, \theta)$ of Lagrangian coordinates, can conventionally be referred to as *rigid model*. The three-by-three mass and stiffness matrices of the rigid model read

$$\mathbf{M}_r = \begin{bmatrix} 1+\Sigma_\varrho^2 & 0 & -2\beta\Delta_{\varrho x}^2 \\ 0 & 1+\Sigma_\varrho^2 & 2\Delta_{\varrho y}^2 \\ -2\beta\Delta_{\varrho x}^2 & 2\Delta_{\varrho y}^2 & \chi^2+\Sigma_\theta^2 \end{bmatrix}, \tag{8}$$

$$\mathbf{K}_r = \begin{bmatrix} \Sigma_{\kappa x} & 0 & -2\beta\Delta_{\kappa x} \\ 0 & \Sigma_{\kappa y} & 2\Delta_{\kappa y} \\ -2\beta\Delta_{\kappa x} & 2\Delta_{\kappa y} & \Sigma_{\kappa\theta} \end{bmatrix}$$

where the out-of-diagonal matrix terms account for the nondimensional mass and stiffness coupling between the translation and rotation $\mathbf{q}_r$ -components.

The second possibility consists in assuming the diaphragm less stiff in its own plane so that the internal constraints of perfect rigidity between the central node and the peripheral nodes can be relaxed. Consequently, the shear-mode deformability is admitted in the mechanical model (the corresponding twelve-by-four constraint matrix $\mathbf{V}_d$ is reported in Appendix A.1). The resulting constrained model, characterized by the four-by-one vector $\mathbf{q}_d = (u, v, \theta, \Gamma)$ of Lagrangian coordinates, conventionally referred to as *deformable model*. The four-by-four mass and stiffness matrices of the deformable model read

$$\mathbf{M}_d = \begin{bmatrix} 1+\Sigma_\varrho^2 & 0 & -2\beta\Delta_{\varrho x}^2 & \beta\Delta_{\varrho x}^2 \\ 0 & 1+\Sigma_\varrho^2 & 2\Delta_{\varrho y}^2 & \beta\Delta_{\varrho y}^2 \\ -2\beta\Delta_{\varrho x}^2 & 2\Delta_{\varrho y}^2 & \chi^2+\Sigma_\theta^2 & 0 \\ \beta\Delta_{\varrho x}^2 & \beta\Delta_{\varrho y}^2 & 0 & \frac{1}{4}\beta^2(\chi^2+\Sigma_\theta^2) \end{bmatrix},$$
$$\mathbf{K}_d = \begin{bmatrix} \Sigma_{\kappa x} & 0 & -2\beta\Delta_{\kappa x} & \beta\Delta_{\kappa x} \\ 0 & \Sigma_{\kappa y} & 2\Delta_{\kappa y} & \beta^2\Delta_{\kappa y} \\ -2\beta\Delta_{\kappa x} & 2\Delta_{\kappa y} & \Sigma_{\kappa\theta} & \beta^2\Delta_{\kappa xy} \\ \beta\Delta_{\kappa x} & \beta^2\Delta_{\kappa y} & \beta^2\Delta_{\kappa xy} & \beta_\Gamma\kappa_s+\Sigma_{\kappa\Gamma} \end{bmatrix} \quad (9)$$

where the out-of-diagonal matrix terms account for the nondimensional mass and stiffness coupling among the two translation, the rotation and the deformation $\mathbf{q}_r$ - components.

It may be worth remarking that the deformable model can be considered an extension of the rigid model, since the mass and stiffness matrices $\mathbf{M}_r$ and $\mathbf{K}_r$ can be recognized as submatrices of the matrices $\mathbf{M}_d$ and $\mathbf{K}_d$. The following auxiliary quantities have been introduced in the mass and stiffness matrices

$$\begin{aligned} \Sigma_\varrho^2 &= \varrho_1^2+\varrho_2^2+\varrho_3^2+\varrho_4^2, \\ \Sigma_\theta^2 &= (1+\beta^2)\Sigma_\varrho^2, \\ \Delta_{\varrho x}^2 &= \frac{1}{2}(\varrho_1^2+\varrho_2^2-\varrho_3^2-\varrho_4^2), \\ \Delta_{\varrho y}^2 &= \frac{1}{2}(\varrho_1^2-\varrho_2^2-\varrho_3^2+\varrho_4^2), \\ \Sigma_{\kappa x} &= \kappa_{x1}+\kappa_{x2}+\kappa_{x3}+\kappa_{x4}, \\ \Sigma_{\kappa y} &= \kappa_{y1}+\kappa_{y2}+\kappa_{y3}+\kappa_{y4}, \\ \Delta_{\kappa x} &= \frac{1}{2}(\kappa_{x1}+\kappa_{x2}-\kappa_{x3}-\kappa_{x4}), \\ \Delta_{\kappa y} &= \frac{1}{2}(\kappa_{y1}-\kappa_{y2}-\kappa_{y3}+\kappa_{y4}), \\ \Sigma_{\kappa\theta} &= \Sigma_{\kappa y}+\beta^2\Sigma_{\kappa x}, \\ \Sigma_{\kappa\Gamma} &= \frac{1}{4}\beta^2(\Sigma_{\kappa x}+\beta^2\Sigma_{\kappa y}), \\ \beta_\Gamma &= 2\beta^2(1+\beta^2), \\ \Delta_{\kappa xy} &= \frac{1}{2}(\Sigma_{\kappa y}-\Sigma_{\kappa x}) \end{aligned} \quad (10)$$

where $(1+\beta^2)$ can be recognized as the nondimensional semi-diagonal of the rectangular diaphragm.

2.2 Direct modal analysis

Denoting by Ω and $\omega = \Omega/\Omega_r$ the dimensional and nondimensional circular frequencies, the free dynamics of the diaphragm can be analyzed by imposing a monoharmonic solution $\mathbf{q} = \boldsymbol{\phi}\exp(\iota\omega\tau)$ in the homogeneous form of the equation of motion (7). Therefore, eliminating the ubiquitous time-dependence, a linear eigenproblem can be stated in the so-called *non-standard* form

$$(\mathbf{K}_q - \lambda\mathbf{M}_q)\boldsymbol{\phi} = \mathbf{0} \quad (11)$$

where the eigensolutions are the real-valued eigenvalues $\lambda = \omega^2$ (or angular square frequencies) and the associated eigenvectors $\boldsymbol{\phi}$ (mode shapes or simply modes).

Depending on the model dimension n, the rigid and the deformable models of the diaphragm are characterized by n = 3 and n = 4 eigenpairs (λ, $\boldsymbol{\phi}$), respectively. The set of eigenvalues $\boldsymbol{\Lambda} = (\lambda_1, \dots, \lambda_h, \dots, \lambda_n)$, sorted in ascending order, constitutes the model spectrum. The matrix $\boldsymbol{\Phi} = [\boldsymbol{\phi}_1, \dots, \boldsymbol{\phi}_h, \dots, \boldsymbol{\phi}_n]$ collecting column-wise the associated modes is the modal matrix. Due to the low model dimension, a closed form solution exists for all the eigenvalues $\lambda(\boldsymbol{\mu})$ of the spectrum $\boldsymbol{\Lambda}(\boldsymbol{\mu})$, and for all the eigenvectors $\boldsymbol{\phi}(\boldsymbol{\mu})$ of the matrix $\boldsymbol{\Phi}(\boldsymbol{\mu})$, as explicit – although non polynomial – function of the parameter vector $\boldsymbol{\mu}$.

From the qualitative viewpoint, if one of the eigencomponents dominates over the others, the eigenvector can be classified as *translation mode* (dominated by the components u and v), *rotation mode* (dominated by the component θ) and *shear mode* (dominated by the component Γ, only for the deformable model). Furthermore, particular parameter combinations can determine eigenvectors participated by two or more eigencomponents in a comparable manner, which can be referred to as *hybrid modes*. From the quantitative viewpoint, the assessment of the modal hybridization can be based on the energy-based asymptotically approximate definition of a modal localization factor (Lepidi and Gattulli 2014).

2.3 Inverse modal analysis

Although undoubtedly valuable to carry out wide parametric analyses, the explicit functions $\boldsymbol{\Lambda}(\boldsymbol{\mu})$ and $\boldsymbol{\Phi}(\boldsymbol{\mu})$ are seldom employable in solving inverse spectral problems of parametric identification. Indeed, parametric identification typically consists in searching for an unknown parameter set $\boldsymbol{\mu}^*$ (output) describing a particular dynamic model characterized by a certain spectrum $\boldsymbol{\Lambda}^*$ and/or a certain modal matrix $\boldsymbol{\Phi}^*$, where all or part of the eigenvalues λ^* and eigenvectors $\boldsymbol{\phi}^*$ are known experimentally (input). In this respect, it may be worth remarking that parametric identification is an advanced issue (second-level structural identification problem) that differs from modal identification. Specifically, parametric identification *starts from* the experimental knowledge of modal information, for instance as the outcome of ambient

vibration tests and operational modal analyses (first-level modal identification problem). Assuming – for the sake of simplicity – that the experimental knowledge is limited to the spectrum $\mathbf{\Lambda}^*$, the exact analytical solution of the parametric identification problem would require the mathematical inversion of the function $\mathbf{\Lambda}(\boldsymbol{\mu})$, in order to solve the equation $\mathbf{\Lambda}(\boldsymbol{\mu}) = \mathbf{\Lambda}^*$. On the one hand, from the mathematical viewpoint, the frequent insufficiency or not-completeness of data tends to compromise the well-posedness of the problem, while the inherent nonlinearity of the governing equations does not guarantee the existence and uniqueness of the solution, in the general case. On the other hand, from the operative viewpoint, the non-polynomial nature of the functions $\mathbf{\Lambda}(\boldsymbol{\mu})$ and $\mathbf{\Phi}(\boldsymbol{\mu})$ reduces the possibility to achieve the analytical solution of the inverse eigenproblem, expressing the unknown $\boldsymbol{\mu}^*$ as an explicit function of the data $\mathbf{\Lambda}^*$.

Within this challenging scenario, it may be worth approaching the modal problem from a slightly different perspective. Specifically, building up uniformly valid and convergent series approximations of the eigenvalues and eigenvectors may allow a sufficiently accurate description of the exact spectrum $\mathbf{\Lambda}$ and modal matrix $\mathbf{\Phi}$, by virtue of polynomial functions of the parameters. Furthermore, low-order polynomial functions are more suitable to be analytically inverted. In general, a well-balanced equilibrium can be found between the competing requirements of: (i) approximation accuracy in the direct modal problem, calling for high-order approximations, and (ii) availability of analytical solutions for the inverse identification problem, calling for low-order approximations. Multi-parametric perturbation methods are the proper mathematical tool to build up the necessary series approximations of the eigensolutions.

2.3.1 Multiparameter perturbation method

Perturbation methods are asymptotic techniques that are widely used to perform eigensolution sensitivity analyses in a variety of scientific research fields, ranging from parametric design and spectral optimization to nonlinear modal identification, damping and damage detection, dynamic stability and bifurcation (Hajj *et al*. 2000, Kerschen *et al*. 2006, Lee *et al*. 2010, Lacarbonara *et al*. 2016, Lofrano *et al*. 2016, Lepidi and Bacigalupo 2018). A general multiparametric perturbation technique for the eigensensitivity analysis of a discrete conservative dynamic system is presented in the following. Therefore, in the next paragraph, the technique is specifically applied to the deformable diaphragm model to the purpose of structural identification and model updating.

The preliminary requirement is that the structural matrices $\mathbf{K}_d(\mathbf{p})$ and $\mathbf{M}_d(\mathbf{p})$ governing the mechanical model are analytical functions of a finite set $\mathbf{p}$ of independent nondimensional parameters (which generally coincides with $\boldsymbol{\mu}$, but can also include suited combinations of the $\boldsymbol{\mu}$-components, if more convenient). In extreme synthesis, the methodological strategy consists in fixing a starting (known) set $\mathbf{p}^\circ$ of parameters, corresponding to an *unperturbed* (or *ideal*) mechanical model governed by the $\mathbf{p}^\circ$-dependent matrices $\mathbf{K}_d^\circ$ and $\mathbf{M}_d^\circ$ and characterized by a known spectrum $\mathbf{\Lambda}^\circ$ and known modal matrix $\mathbf{\Phi}^\circ$. The starting set $\mathbf{p}^\circ$ can be determined on the base of an order of magnitude analysis or by solving an inverse spectral problem (Lepidi 2013). Therefore, the generic *real* (non-ideal) mechanical models corresponding to the parameter set $\mathbf{p}$ is assumed as *perturbation* of the ideal mechanical model, originated by a small change in a generic direction $\mathbf{p}'$ of the parameter space (namely a *multiparameter perturbation*). The smallness of the multiparameter perturbation is regulated by a so-called *ordering* rule that – in the simplest case – can be introduced in the form

$$\mathbf{p} = \mathbf{p}^\circ + \epsilon\mathbf{p}' \tag{12}$$

where $\epsilon \ll 1$ is a small nondimensional parameter measuring the geometric distance between the ideal and the real mechanical models in the parameter space. Although not strictly necessary for pointing out the mathematical algorithm in the following, higher order perturbation schemes $\mathbf{p} = \mathbf{p}^\circ + \epsilon\mathbf{p}' + \epsilon^2\mathbf{p}'' + \dots$ could be considered, without conceptual difficulties. Naturally, all and only the real mechanical models corresponding to the parameter sets $\mathbf{p}$, encircled in a small-radius hypersphere of the parameter space centered at the starting set $\mathbf{p}^\circ$, can be described. Imposing the parameter ordering, the governing matrices $\mathbf{K}_d(\mathbf{p})$ and $\mathbf{M}_d(\mathbf{p})$ can be expanded in integer ϵ power series

$$\begin{aligned}
\mathbf{K}_d &= \mathbf{K}_d^\circ + \sum_n \epsilon^n \mathbf{K}_d^{(n)} \\
&= \mathbf{K}_d^\circ + \epsilon\mathbf{K}_d' + \epsilon^2\mathbf{K}_d'' + \epsilon^3\mathbf{K}_d''' + \epsilon^4\mathbf{K}_d'''' + \cdots \\
\mathbf{M}_d &= \mathbf{M}_d^\circ + \sum_n \epsilon^n \mathbf{M}_d^{(n)} \\
&= \mathbf{M}_d^\circ + \epsilon\mathbf{M}_d' + \epsilon^2\mathbf{M}_d'' + \epsilon^3\mathbf{M}_d''' + \epsilon^4\mathbf{M}_d'''' + \cdots
\end{aligned} \tag{13}$$

where the unperturbed matrices $\mathbf{K}_d^\circ$ and $\mathbf{M}_d^\circ$ tend to be sparse or even diagonal, if the set $\mathbf{p}^\circ$ is properly selected. The perturbation matrices $\mathbf{K}_d^{(n)}$ and $\mathbf{M}_d^{(n)}$ are symmetric at each ϵ-order and are known functions of the sets $\mathbf{p}^\circ$ and $\mathbf{p}'$ of mechanical parameters.

The symmetry of the stiffness and mass matrices $\mathbf{K}_d^\circ$ and $\mathbf{M}_d^\circ$ ensures that the spectrum $\mathbf{\Lambda}^\circ$ does not include defective eigenvalues. Therefore, it is possible to postulate that the eigenvalues and eigenvectors can be expressed as integer ϵ-power series in the form

$$\begin{aligned}
\lambda &= \lambda^\circ + \sum_n \epsilon^n \lambda^{(n)} \\
&= \lambda^\circ + \epsilon\lambda' + \epsilon^2\lambda'' + \epsilon^3\lambda''' + \epsilon^4\lambda'''' + \cdots, \\
\boldsymbol{\phi} &= \boldsymbol{\phi}^\circ + \sum_n \epsilon^n \boldsymbol{\phi}^{(n)} \\
&= \boldsymbol{\phi}^\circ + \epsilon\boldsymbol{\phi}' + \epsilon^2\boldsymbol{\phi}'' + \epsilon^3\boldsymbol{\phi}''' + \epsilon^4\boldsymbol{\phi}'''' + \cdots
\end{aligned} \tag{14}$$

where the coefficients $\lambda^{(n)}$ and $\boldsymbol{\phi}^{(n)}$ represent the n-th *sensitivities* of the eigenvalues and eigenvectors, respectively. The n-th sensitivities of the eigenvalues and eigenvectors are collected in the vector $\mathbf{\Lambda}^{(n)}$ and matrix

$\boldsymbol{\Phi}^{(n)}$, which can be also referred to as *eigensensitivities*. According to the multiparameter perturbation method, the eigensensitivities are the *unknowns* of the modal problem.

Imposing both the series expansions (13) of the data (governing matrices $\mathbf{K}_d^\circ$ and $\mathbf{M}_d^\circ$ and their perturbations) and the series expansions (14) of the unknowns (eigenvalues and eigenvectors *sensitivities*) in the eigenvalue problem, expanding and collecting terms of the same ϵ-power, an ϵ-ordered cascade of *perturbation equations* can be formulated

$$\begin{aligned}
&\epsilon^0 : \left(\mathbf{K}_d^\circ - \lambda^\circ \mathbf{M}_d^\circ\right)\boldsymbol{\phi}^\circ = \mathbf{0} \\
&\epsilon^1 : \left(\mathbf{K}_d^\circ - \lambda^\circ \mathbf{M}_d^\circ\right)\boldsymbol{\phi}' = -\left(\mathbf{K}_d' - \lambda^\circ \mathbf{M}_d' - \lambda' \mathbf{M}_d^\circ\right)\boldsymbol{\phi}^\circ \\
&\epsilon^2 : \left(\mathbf{K}_d^\circ - \lambda^\circ \mathbf{M}_d^\circ\right)\boldsymbol{\phi}'' \\
&\quad = -\left(\mathbf{K}_d'' - \lambda^\circ \mathbf{M}_d'' - \lambda' \mathbf{M}_d' - \lambda'' \mathbf{M}_d^\circ\right)\boldsymbol{\phi}^\circ \\
&\quad\quad -\left(\mathbf{K}_d' - \lambda^\circ \mathbf{M}_d' - \lambda' \mathbf{M}_d^\circ\right)\boldsymbol{\phi}' \\
&\ldots : \ldots \\
&\epsilon^n : \left(\mathbf{K}_d^\circ - \lambda^\circ \mathbf{M}_d^\circ\right)\boldsymbol{\phi}^{(n)} \\
&\quad = -\left(\mathbf{K}_d^{(n)} - \sum_{j=0}^{n} \lambda^{(j)} \mathbf{M}_d^{(n-j)}\right)\boldsymbol{\phi}^\circ \\
&\quad\quad -\sum_{k=1}^{n-1}\left[\left(\mathbf{K}_d^{(k)} - \sum_{j=0}^{k} \lambda^{(j)} \mathbf{M}_d^{(k-j)}\right)\boldsymbol{\phi}^{(n-k)}\right]
\end{aligned} \tag{15}$$

where the equation at the ϵ^0-order can be recognized to govern the eigenproblem of the ideal mechanical model. The corresponding *generating* eigensolution is known by hypothesis and composed by the generating eigenvalues λ_h° of the spectrum $\boldsymbol{\Lambda}^\circ$ and the associated generating eigenvectors $\boldsymbol{\phi}_h^\circ$ of the modal matrix $\boldsymbol{\Phi}^\circ$ (with $h = 1, \ldots, n$). All the generating eigenvalues λ_h° are supposed to be simple (characterized by unitary algebraic multiplicity) and well separated (that is, the difference between any two eigenvalues is supposed to be at least one order of magnitude greater than ϵ).

The key assumption of simplicity and well-separation of the n-th generating eigenvalue determined at the lowest order (namely ϵ^0-order) ensures that each higher order (namely ϵ^n-order with $n \geq 1$) of the perturbation equations allows to determine the n-th sensitivity $\lambda_h^{(n)}$ of the h-th eigenvalue and the n-th sensitivity $\boldsymbol{\phi}_h^{(n)}$ of the h-th eigenvector. Specifically, the n-th eigenvalue sensitivity $\lambda_h^{(n)}$ is determined by imposing the solvability condition of the ϵ^n-order Eq. (15d), yielding

$$\begin{aligned}
\lambda_h^{(n)} = \alpha_h^\circ \boldsymbol{\phi}_h^{\circ\top}&\left(\mathbf{K}_d^{(n)} - \sum_{j=0}^{n-1} \lambda_h^{(j)} \mathbf{M}_d^{(n-j)}\right)\boldsymbol{\phi}_h^\circ \\
&+\alpha_h^\circ \sum_{k=1}^{n-1}\left[\boldsymbol{\phi}_h^{\circ\top}\left(\mathbf{K}_d^{(k)} - \sum_{j=0}^{k} \lambda_h^{(j)} \mathbf{M}_d^{(k-j)}\right)\boldsymbol{\phi}_h^{(n-k)}\right]
\end{aligned} \tag{16}$$

where $\alpha^\circ = (\boldsymbol{\phi}^{\circ\top} \mathbf{M}_d^\circ \boldsymbol{\phi}^\circ)^{-1}$. From the technical viewpoint, the solvability has been imposed by requiring the orthogonality between the right-hand term of Eq. (15d) and the solution $\boldsymbol{\psi}_h$ of the auxiliary homogeneous problem $(\mathbf{K}_d^\circ - \lambda^\circ \mathbf{M}_d^\circ)^\top \boldsymbol{\psi} = \mathbf{0}$, according to the Fredholm Alternative for discrete linear systems. Furthermore, the identity $\boldsymbol{\psi}_h = \boldsymbol{\phi}_h^\circ$ has been employed, as long as the symmetry of the matrices $\mathbf{K}_d^\circ$ and $\mathbf{M}_d^\circ$ holds. Once the n-th eigenvalue sensitivity $\lambda_h^{(n)}$ is known, the n-th eigenvector sensitivity $\boldsymbol{\phi}_h^{(n)}$ is univocally determined

$$\begin{aligned}
\boldsymbol{\phi}_h^{(n)} = -\mathbf{A}_h^\circ &\left[\mathbf{A}_h^{\circ\top}\left(\mathbf{K}_d^\circ - \lambda_h^\circ \mathbf{M}_d^\circ\right)\mathbf{A}_h^\circ\right]^{-1} \\
&\sum_{k=1}^{n}\left[\mathbf{A}_h^{\circ\top}\left(\mathbf{K}_d^{(k)} - \sum_{j=0}^{k} \lambda_h^{(j)} \mathbf{M}_d^{(k-j)}\right)\boldsymbol{\phi}_h^{(n-k)}\right]
\end{aligned} \tag{17}$$

where the rectangular matrix $\mathbf{A}_h^\circ = [\boldsymbol{\phi}_1^\circ, \ldots, \boldsymbol{\phi}_{i \neq h}^\circ, \ldots, \boldsymbol{\phi}_N^\circ]$ is obtained by removing the h-th eigenvector from the modal matrix $\boldsymbol{\Phi}^\circ$. From the technical viewpoint, the n-th sensitivity of the h-th eigenvector has been expressed as a linear combination of all the i-th eigenvectors $\boldsymbol{\phi}_i^\circ$ (with $i \neq h$), with small (n-th order) combination coefficients (Lepidi 2013).

From the mathematical viewpoint, determining the n-th sensitivities $\lambda_h^{(n)}$ and $\boldsymbol{\phi}_h^{(n)}$ allows the analytical assessment of all the coefficients of the power series (14) and, therefore, the asymptotic reconstruction of the eigenvalue and eigenvector up to the desired approximation order. The reconstruction procedure implies the complete reabsorption of the ϵ-parameter. From the mechanical viewpoint, Eqs. (16) and (17) allow to obtain closed-form expressions of the frequencies and modes of a discrete system as analytical – although asymptotically approximate – functions of the parameters. As a major remark, the multiparameter perturbation method and the analytical formulas (16) and (17) are completely general, since they hold for any mechanical non-dissipative linear discrete system possessing a generic number of degrees-of-freedom and described by a generic number of parameters. It may be worth recalling that – coherently with the nature of perturbation techniques – the accuracy of the eigensolution approximations depends on the maximum order of the series, while its mathematical consistency holds within the limits of the parameter smallness assumptions and within the convergence radius of the power series.

Finally, it is worth to briefly address the advantages and potential drawbacks of the proposed perturbation approach in the field of model updating. If compared, for example, to the well-studied sensitivity method in finite element model updating (Jaishi and Ren 2005, Reynders *et al*. 2010, Mottershead *et al*. 2011), the leading concept is quite similar. The linearization of the problem – being it an eigenvalue or an optimization problem – is exploited to formulate more simple and manageable inverse relationships. In this respect, the perturbative derivation has the benefit to identify a solution in a proper analytical form, within the space of the low-dimensional mass and stiffness matrices of the direct model. Indeed, the few parameters describing the model can be identified without recurring to numerical optimization schemes. On the downside, the flexibility of the approach relies on the possibility to describe the actual structural behavior through a low-fidelity model, as discussed in the following with respect to

the experimental applications.

2.3.2 Parameter identification and model updating

To the purpose of the parameter identification problem, the multiparameter perturbation method allows determining the parametric relations $\boldsymbol{\Lambda}(\boldsymbol{\mu})$ and $\boldsymbol{\Phi}(\boldsymbol{\mu})$ (or equivalently $\boldsymbol{\Lambda}(\mathbf{p})$ and $\boldsymbol{\Phi}(\mathbf{p})$), required to state the inverse spectral problem. It is important to highlight that – according to the multiparameter perturbation method – the power series approximations of the eigenvalues and eigenvectors are polynomial functions of the ϵ parameter regulating the amplitude of the multiparameter perturbation $\mathbf{p}'$, whereas they remain non-polynomial functions of each $\mathbf{p}'$-component, in the general case. Therefore, the invertibility of the spectral problem must be discussed at each order of approximation.

In order to specify the multiparameter perturbation method for the deformable model of the planar diaphragm, it is first necessary to select and order of the parameter set $\mathbf{p}$. Its selection is a key technical point, because the perturbation-based inversion of the modal problem – if mathematically feasible – does not allow to identify unknown parameters other than those included in the set $\mathbf{p}$. For the deformable model, a suited set of independent parameters is $\mathbf{p} = (\beta,\ \chi^2,\ \kappa_s,\ \Sigma_\varrho^2,\ \Sigma_{\kappa x},\ \Sigma_{\kappa y},\ \Delta_{\varrho x}^2,\ \Delta_{\varrho y}^2,\ \Delta_{\kappa x},\ \Delta_{\kappa y})$, sufficient to completely and univocally assess the mass and stiffness matrices (9). Relying on engineering considerations, a proper ϵ-power ordering of the $\mathbf{p}$-components is

$$\begin{aligned}
&\beta = \beta_0, && \chi^2 = \chi_0^2 + \epsilon\chi_1^2, && \Sigma_\varrho^2 = \Sigma_{\varrho 0}^2,\\
&\Delta_{\varrho x}^2 = \epsilon\Delta_{\varrho x1}^2, && \Delta_{\varrho y}^2 = \epsilon\Delta_{\varrho y1}^2, &&\\
&\kappa_s = \kappa_{s0} + \epsilon\kappa_{s1}, && \Sigma_{\kappa x} = \Sigma_{\kappa x0}, && \Sigma_{\kappa y} = \Sigma_{\kappa y0},\\
&\Delta_{\kappa x} = \epsilon\Delta_{\kappa x1}, && \Delta_{\kappa y} = \epsilon\Delta_{\kappa y1} &&
\end{aligned} \tag{18}$$

where the subscript indicates the ϵ-order of the parameter perturbation. Thus, it is consistent to assume the dependent parameter $\Delta_{\kappa xy}$ to be ordered as $\Delta_{\kappa xy} = \epsilon\Delta_{\kappa xy1}$. After substituting the parameter ordering (18) in the mass and stiffness matrices $\mathbf{M}_d$ and $\mathbf{K}_d$ reported in Eq. (9), expanding and collecting terms of the same ϵ-power, the matrix expansions (13) can be specified for the deformable diaphragm. The unperturbed matrices $\mathbf{M}_d^\circ$ and $\mathbf{K}_d^\circ$ (depending on the zeroth-order parameters only) and the first perturbation matrices $\mathbf{M}_d'$ and $\mathbf{K}_d'$ are reported in Appendix A.2. From the physical viewpoint, the matrices $\mathbf{M}_d^\circ$ and $\mathbf{K}_d^\circ$ collect the dominant contributions to the model mass and stiffness, whereas the perturbation matrices $\mathbf{M}_d'$ and $\mathbf{K}_d'$ collect minor or minimal contributions to the model mass and stiffness, consistently with the perturbation approach.

Some brief remarks can be pointed out to specify the technical range of structural samples satisfying the particular order assignment (18). First, square and rectangular diaphragms are considered (namely, from the mathematical viewpoint, rectangles with aspect ratio $\beta = \mathcal{O}(1)$). Second, diaphragms with non-negligible rotational inertia are taken into account (rotational-to-translational mass ratio $\chi^2 = \mathcal{O}(1)$). Third, non-rigid but stiff diaphragms are assumed (shear stiffness $\kappa_s = \mathcal{O}(1)$). Finally, mass and stiffness eccentricities are certainly admitted, as long as they are not dominant (mass differences $\Delta_{\varrho x}^2 = \mathcal{O}(\epsilon)$, $\Delta_{\varrho y}^2 = \mathcal{O}(\epsilon)$ and stiffness differences $\Delta_{\kappa x} = \mathcal{O}(\epsilon)$, $\Delta_{\kappa y} = \mathcal{O}(\epsilon)$). It is worth remarking that different parameter orderings can equally be introduced, if necessary to describe other structural cases falling out of this parameter range (for instance, highly elongated rectangular diaphragms).

Following the general strategy outlined for the multiparameter perturbation method, the zeroth-order analytical approximation of the model spectrum $\boldsymbol{\Lambda}^\circ = (\lambda_1^\circ, \lambda_2^\circ, \lambda_3^\circ, \lambda_4^\circ)$ can be univocally determined. Specifically, the four generating eigenvalues and the corresponding eigenvectors are

$$\begin{aligned}
&\lambda_1^\circ = \frac{\Sigma_{\kappa x}}{1+\Sigma_\varrho^2}, && \boldsymbol{\phi}_1^\circ = (1,0,0,0)\\
&\lambda_2^\circ = \frac{\Sigma_{\kappa y}}{1+\Sigma_\varrho^2}, && \boldsymbol{\phi}_2^\circ = (0,1,0,0)\\
&\lambda_3^\circ = \frac{\Sigma_{\kappa\theta}}{\chi_0^2+\Sigma_\theta^2}, && \boldsymbol{\phi}_3^\circ = (0,0,1,0)\\
&\lambda_4^\circ = \frac{4\left(\beta_\Gamma\kappa_{s0}+\Sigma_{\kappa\Gamma}\right)}{\beta^2\left(\chi_0^2+\Sigma_\theta^2\right)}, && \boldsymbol{\phi}_4^\circ = (0,0,0,1)
\end{aligned} \tag{19}$$

where all the eigenvectors can be recognized to be canonical vectors with unitary-amplitude, meaning that zeroth order modes of the deformable system are perfectly localized on one or the other degrees-of-freedom. The first eigenvalue sensitivities are

$$\begin{aligned}
&\lambda_1' = 0\\
&\lambda_2' = 0\\
&\lambda_3' = -\frac{\chi_1^2\Sigma_{\kappa\theta}}{\left(\chi_0^2+\Sigma_\theta^2\right)^2}\\
&\lambda_4' = \frac{4\beta_\Gamma\kappa_{s1}(\chi_0^2+\Sigma_\theta^2) - 4\beta_\Gamma\kappa_{s0}\chi_1^2 - 4\Sigma_{\kappa\Gamma}\chi_1^2}{\beta^2\left(\chi_0^2+\Sigma_\theta^2\right)^2}
\end{aligned} \tag{20}$$

Higher (second, third) sensitivities could be determined up to the desired approximation order. It may be worth remarking that the lowest order significant perturbation of the eigenvalues λ_1 and λ_2 is given by the second sensitivities λ_1'' and λ_2'', because the first sensitivities λ_1' and λ_2' are identically null. The accuracy of the power-series approximation (14), reconstructed up to the second order by employing the generating eigenvalues (19) and the sensitivities (20), must be discussed from a direct comparison with the exact eigenvalues. Particularly, the qualitative and quantitative agreement between the approximate and exact eigenvalues under variation of the perturbation parameter ϵ can be appreciated in Fig. 2 for two different multiparameter perturbations. The multiparameter perturbations are purposely selected to introduce small (ϵ-proportional) variations of the mass and stiffness matrices, respectively. The approximate solution appears quite accurate with respect to mass perturbations (Fig. 2(a)), since it closely matches the exact solution. Remarkably, the agreement between the approximate and

(a) Mass perturbations (b) Stiffness perturbations

Fig. 2 Comparison between the exact and approximate eigenvalue loci (normalized with respect to the unperturbed eigenvalue) versus ϵ-proportional perturbations of (a) the mass matrix; (b) the stiffness matrix of the deformable diaphragm (parameters $\beta = \frac{2}{3}, \chi^2 = \frac{1}{4}, \kappa_s = \frac{1}{3}, \Sigma_\varrho^2 = 9, \Sigma_{\kappa x} = 2, \Sigma_{\kappa y} = 1, \Delta_{\varrho x}^2 = \frac{1}{4}, \Delta_{\varrho y}^2 = \frac{1}{9}, \Delta_{\kappa x} = \frac{1}{4}, \Delta_{\kappa y} = \frac{1}{5}$)

exact solutions persists even beyond the expected range of accuracy (namely $\epsilon \ll 1$, according the initial hypothesis of the perturbation method). The approximate solution turns out to be satisfyingly accurate for stiffness perturbations as well (Fig. 2(b)), even if the larger sensitivity of some eigenvalues slightly reduce the approximation accuracy (for ϵ approaching unity).

Recalling the modal formulation outlined at the beginning of Section 2.3, the parameter identification problem consists in inverting the analytical equation $\mathbf{\Lambda}(\boldsymbol{\mu}) = \mathbf{\Lambda}^*$ in order to determine the mechanical parameter set $\boldsymbol{\mu}$ (or $\mathbf{p}$) corresponding to the experimental spectrum $\mathbf{\Lambda}^*$. For the deformable diaphragm model, the problem can be solved straightforwardly by recognizing that the analytical expressions (19) of the generating eigenvalues linearly depend – with a direct or inverse relationship – on the unperturbed mass and stiffness parameters. Similarly, the analytical expressions (20) of the eigenvalue sensitivities depend on the mass and stiffness perturbations. Therefore, by virtue of the multiparameter perturbation method, Eqs. (19) and (20) are simple analytical relations in the form $\mathbf{\Lambda}(\mathbf{p})$, suited to be easily inverted to determine the diaphragm mass and stiffness $\mathbf{p}$-parameters that (approximately) correspond to a certain experimental spectrum $\mathbf{\Lambda}^* = (\lambda_1^*, \lambda_2^*, \lambda_3^*, \lambda_4^*)$.

Considering the availability of four zeroth-order equations for the generating eigenvalues and four higher-order equations for the lowest-order eigenvalue perturbations (given by the second sensitivities λ_1'' and λ_2'' for the eigenvalues λ_1 and λ_2 and by the first sensitivities λ_3' and λ_4' for the eigenvalues λ_3 and λ_4), the identification problem can be targeted at identifying no more than eight unknowns selected in the set of all the unperturbed parameters and/or parameter perturbations. Consequently, the balance of data and unknowns states that some mechanical parameters must be considered known a priori. Among the other possibilities, engineering considerations suggest assuming – with all likelihood – the aspect ratio β and the masses Σ_ϱ^2, $\Delta_{\varrho x1}^2$, $\Delta_{\varrho y1}^2$ as known information.

Based on the above conceptual framework and practical assumptions, the *parameter identification* consists in determining the unknown zeroth-order stiffnesses $\Sigma_{\kappa x}$ and $\Sigma_{\kappa y}$, rotational mass χ_0^2, and shear stiffness κ_{s0} of the deformable diaphragm model by (i) imposing the coincidence between the zeroth-order analytical approximation of the model spectrum $\mathbf{\Lambda}^\circ$ and the experimental spectrum $\mathbf{\Lambda}^*$ (namely $\lambda_i^\circ = \lambda_i^*$ for i = 1, …, 4), and (ii) analytically inverting Eq. (19), yielding

$$\begin{aligned}
\Sigma_{\kappa x} &= \omega_1^{*2}\left(1 + \Sigma_\varrho^2\right) \\
\Sigma_{\kappa y} &= \omega_2^{*2}\left(1 + \Sigma_\varrho^2\right) \\
\chi_0^2 &= \frac{(\beta^2\omega_1^{*2} + \omega_2^{*2})\left(1 + \Sigma_\varrho^2\right) - \omega_3^{*2}\Sigma_\theta^2}{\omega_3^{*2}} \\
\kappa_{s0} &= \frac{\beta^2\omega_4^{*2}(\beta^2\omega_1^{*2} + \omega_2^{*2})\left(1 + \Sigma_\varrho^2\right)}{4\beta_\Gamma\omega_3^{*2}} \\
&\quad - \frac{\beta^2\omega_3^{*2}(\omega_1^{*2} + \beta^2\omega_2^{*2})\left(1 + \Sigma_\varrho^2\right)}{4\beta_\Gamma\omega_3^{*2}}
\end{aligned} \tag{21}$$

where ω_1^*, ω_2^*, ω_3^*, ω_4^* are the – adimensionalized, $\omega_i^* = \Omega_i^*/\Omega_r$ – experimental circular frequencies (square roots of the eigenvalues), coming out from operational modal analyses. It may be worth noting that the identified zero-order parameters do not depend on the first order (known) parameters accounting for the mass eccentricities $\Delta_{\rho x1}^2, \Delta_{\rho y1}^2$. The one-to-one association of the i-th experimental frequency ω_i^* with the i-th generating eigenvalue λ_i° can be governed by any assurance criterion suited to associate the generating eigenvectors with the corresponding experimental mode shapes.

The parameter identification suffices to assess a zeroth-order structural model of the deformable diaphragm, governed by the mass matrix $\mathbf{M}_d^\circ$ and stiffness matrix $\mathbf{K}_d^\circ$ generated by the identified parameters (21) and matching exactly the experimental spectrum $\mathbf{\Lambda}^*$. Clearly, the identified structural model cannot be expected to match exactly also the experimental modes $\mathbf{\Phi}^*$, because they have not been involved in the identification process. Once the zeroth-order structural model has been identified, the structural model can further be refined by determining higher order contributions to the mass and stiffness matrices. The model refinements can be required to not alter the coincidence between the analytical approximation of the model spectrum $\mathbf{\Lambda}^\circ + \mathbf{\Lambda}' + \mathbf{\Lambda}''$ and the experimental spectrum $\mathbf{\Lambda}^*$ (namely $\lambda_i^\circ + \lambda_i' + \lambda_i'' = \lambda_i^*$ for i = 1, …, 4).

Therefore, the *model updating* consists in determining the unknown higher-order perturbations (*updates*) of the model stiffnesses $\Delta_{\kappa x1}$ and $\Delta_{\kappa y1}$, rotational mass χ_1^2, and

shear stiffness κ_{s1}. This is obtained by (i) imposing the coincidence between the second-order analytical approximation of the model spectrum $\mathbf{\Lambda}^{\circ} + \mathbf{\Lambda}' + \mathbf{\Lambda}''$ and the experimental spectrum $\mathbf{\Lambda}^{*}$, then (ii) analytically inverting the non-polynomial equations expressing the spectral coincidence (namely $\lambda_i' + \lambda_i'' = 0$ for i = 1, …, 4) to determine the unknown updates $\Delta_{\kappa x1}$, $\Delta_{\kappa y1}$, χ_1^2, κ_{s1} and finally, if the analytical inversion is impossible, (iii) approximate the unknown updates $\Delta_{\kappa x1}$, $\Delta_{\kappa y1}$, χ_1^2, κ_{s1} to the lowest order, consistently with the asymptotic expansion. Following this strategy, the updating reads

$$\begin{aligned} \Delta_{\kappa x1} &= \frac{\Sigma_{\kappa x}\Delta_{\varrho x1}^2}{1+\Sigma_{\varrho}^2} \\ \Delta_{\kappa y1} &= \frac{\Sigma_{\kappa y}\Delta_{\varrho y1}^2}{1+\Sigma_{\varrho}^2} \\ \chi_1^2 &= 0 + \mathcal{O}(\epsilon) \\ \kappa_{s1} &= \frac{\chi_1^2(\beta_\Gamma \kappa_{s0} + \Sigma_{\kappa\Gamma})}{\beta_\Gamma(\chi_0^2 + \Sigma_\theta^2)} + \mathcal{O}(\epsilon) \end{aligned} \tag{22}$$

where it can be recognized that the first order parameters accounting for the stiffness eccentricities $\Delta_{\kappa x1}$, $\Delta_{\kappa y1}$ depend on the first order (known) parameters accounting for the mass eccentricities $\Delta_{\rho x1}^2$, $\Delta_{\rho y1}^2$, as expected. Finally, from the perspective of engineering applications, it is useful to relate the stiffness κ_s of the two cross bracings to the shear stiffness κ_G of a homogeneous plate with in-plane shear modulus G and thickness S. Based on a simple equivalence of elastic energy, this is achieved through the expression

$$\kappa_G = \frac{G_{eq}}{M\Omega_r^2} = \frac{2\beta\kappa_s}{1+\beta^2} \tag{23}$$

where $G_{eq} = GS$ represents the (equivalent) physical stiffness of the diaphragm.

3. Numerical simulations

The actual effectiveness of the theoretical framework and the reliability of the inverse solutions obtained in the previous sections can be firstly verified by employing a structural model of known physical parameters. To this purpose, the pseudo-experimental data are generated by numerically simulating the free oscillations of a computational model describing the linear undamped dynamics of a prototypical simple structure. For the sake of simplicity, the finite element model (named 1S) of a tridimensional one-story, single-bay steel frame with an asymmetric distribution of mass and stiffness is employed (Fig. 3(a)).

The dimension of the rectangular frame plan are 2 m (along the x direction) by 1.5 m (along the y direction) and the inter-story height is equal to 2 m. The four steel columns (HEB 140), oriented with their maximum moment of inertia along the y direction, are rigidly connected at the top by four edge beams (IPE 180). Two additional point masses of 145 kg are added to the vertices of the edge along the x direction, breaking the mass symmetry of the structure. The floor in-plane shear stiffness k_s is provided by two diagonal bracings of varying axial stiffness. In particular, the *rigid*, *semirigid* and *deformable* models considered in the analyses conventionally correspond to the pseudo-experimental frequency f_4^* of the *shear mode* being close (same order of magnitude), far (up to one order larger) or very far (at least one order larger) with respect to the pseudo-experimental rigid modal frequencies f_1^*, f_2^*, f_3^* (Fig. 3(b)). Lastly, concerning the modeling hypotheses, the two-nodes beam elements follow the Euler-Bernoulli theory and the peripheral nodes of the diaphragm are constrained to move in the plane.

Assuming thus the masses of the columns and of the floor beams to be lumped to the diaphragm peripheral nodes (145 kg per node), the geometric and mass parameters read A = 2 m, B = 1.5 m, M = 0 kg, $m_1 = m_2$ = 145 + 145 kg, $m_3 = m_4$ = 145 kg. Employing the natural frequencies provided by the finite element solution of the eigenproblem as pseudo-experimental data, the inverse relationship (21d) allows identifying the zeroth-order approximation of the shear stiffness parameter k_s (Table 1). The results highlight the effectiveness of the procedure in identifying the order of magnitude of k_{s0}, committing – from an engineering point of view – an acceptable overestimation. The difference is at least one order of magnitude smaller than the shear stiffness value and tends to increase the higher the diaphragm deformability. This behavior, however, should be expected and is consistent with the

(a) Model 1S (b) Rigid-body and shear deformability modes

Fig. 3 Scheme of (a) the one-story finite element model 1S, developing (b) two modes dominated by the rigid translation U, V along the x and y directions at frequencies f_1^*, f_2^*, one mode dominated by the rigid rotation θ at frequency f_3^* and one mode dominated by the shear strain Γ at frequency f_4^*

Table 1 Left side: values of the shear stiffness k_s assigned to the rigid, semi-rigid and deformable 1S frame model and corresponding natural frequencies of the rigid (f_1^*, f_2^*, f_3^*) and shear (f_4^*) modes. Right side: values of the zeroth-order k_{s0} shear stiffness approximation structurally identified from the pseudo-experimental frequencies

1S model	k_s (N m^{-1})	f_1^* (Hz)	f_2^* (Hz)	f_3^* (Hz)	f_4^* (Hz)	k_{s0} (N m^{-1})
Rigid	1.00×10^8	24.56	14.16	18.03	156.00	1.09×10^8
Semi-rigid	1.00×10^7	24.12	14.16	17.83	55.46	1.21×10^7
Deformable	1.00×10^6	21.74	14.16	16.38	31.38	3.09×10^6

ϵ-ordering previously assumed for the adimensional shear stiffness κ_s (see Eq. (18)), which is suitable for non-rigid but still stiff diaphragms.

4. Experimental applications

4.1 JetPACS frame

Within an Italian national project targeted at the mitigation of the dynamic response of structures to seismic actions (ReLUIS 2005-2008, Research Line 7), the experimental dynamic testing program JetPACS (Joint Experimental Testing on Passive and semiActive Control Systems) involved the design and construction of a 2/3 scaled steel building prototype aimed at testing active and passive energy dissipation devices for seismic protection (Dolce *et al*. 2008, Gattulli *et al*. 2009). A detailed description of the geometrical and mechanical properties of the two-story, single-bay frame can be found in Ponzo *et al*. (2012). To the purpose of this Section, it is sufficient to mention that the three different mass configurations which were dynamically tested under ambient vibrations, named CB, CS and CN, represent respectively the bare frame (Fig. 4(a)), the double symmetric and non-symmetric added masses arrangements. For the sake of simplicity, the point masses added to the diaphragm (335 kg each) are lumped to the nearest peripheral nodes, together with the column and beam masses (Table 2). Finally, a concrete slab with a mass of around 3000 kg provides an unknown in-plane equivalent shear stiffness $G_{eq} = GS$, where G is the shear modulus of the concrete and S is the diaphragm out-of-plane thickness. A possible energy-based equivalence between k_s and G_{eq} is reported at the end of Section 2.3.2.

Dealing with a multi-story structure, different possibilities are available to carry out the diaphragm stiffness identification. It should be possible, theoretically, to analyze the structure story-by-story, employing only the corresponding experimental measurements and assigning the mass parameters accordingly. However, this approach would face several difficulties in identifying the frequencies and local mode shapes of a particular story. An alternative option, which has been followed in the proposed applications, is to consider the structure as a whole, without employing any additional information (i.e., higher-frequency modes). This choice can be justified both from a structural point of view, since the stories of the analyzed structures present the same mechanical characteristics, and from a conceptual point of view, in order to preserve the straightforwardness of the procedure. Indeed, a slight overestimation of the real diaphragm shear stiffness is expected as a trade-off.

The experimental modes of the frame in each mass configuration have been identified by means of output-only

(a) JetPACS frame, CB configuration

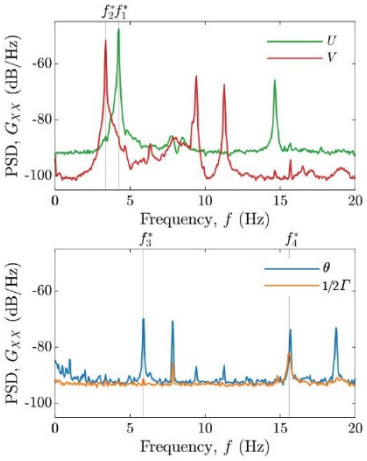

(b) PSD of the rigid translations, rotation and shear strain

Fig. 4 (a) Picture of the JetPACS frame in the bare configuration CB during the ambient vibration testing carried out in the DiSGG structural laboratory of the University of Basilicata. (b) Power spectral densities of the rigid translations U, V, the rigid rotation θ and shear strain Γ (adapted from Sivori *et al*. 2020), estimated from ambient vibration data acquired at the second story of the JetPACS frame (CB configuration)

Table 2 Geometrical and mass properties of the JetPACS frame in the bare (CB), symmetric (CS) and non-symmetric (CN) configurations

JetPACS	A (m)	B (m)	M (kg)	m_1, m_2 (kg)	m_3, m_4 (kg)
CB				2 × 133	2 × 133
CS	2	1.5	2 × 3000	2 × (133 + 335)	2 × (133 + 335)
CN				2 × (133 + 335)	2 × 133

Table 3 Left side: natural frequencies f_1^*, f_2^*, f_3^* of the rigid modes and f_4^* of the shear mode as experimentally identified on the JetPACS frame. Right side: structural identification of the zeroth-order approximation G_{eq0} of the equivalent shear stiffness from experimental frequencies

JetPACS	f_1^* (Hz)	f_2^* (Hz)	f_3^* (Hz)	f_4^* (Hz)	G_{eq0} (N m^{-1})
CB	4.23	3.38	5.89	15.60	2.71×10^6
CS	3.58	2.85	5.11	13.15	2.49×10^6
CN	3.84	3.08	5.51	14.08	2.45×10^6

modal analysis, employing the well-known *frequency domain decomposition* technique (Brincker *et al*. 2001), estimating the *Welch* periodograms with a frequency resolution of 0.01 Hz. Only the signals – 1800 s at a sampling frequency of 200 Hz – coming from two orthogonal pairs of monoaxial accelerometers placed at the opposite corners of each story have been considered, supposing a minimum sensor availability situation which still allows discriminating rigid modes from shear-deformable ones. To this purpose, one of the possible approaches consists in identifying the frequencies of the two rigid translational modes f_1^*, f_2^* from the amplification peaks of the power spectral density (PSD) of the reconstructed rigid translations U, V of the diaphragm centroid. As an example, in the reference (bare) configuration CB, the rigid translation modes in x and y can be identified at 4.23 Hz and 3.38 Hz respectively (top of Fig. 4(b)). Similarly, for what concerns the torsional and the shear modes, they can be identified exploiting the experimental spectra of the rigid rotation θ and shear strain Γ (Sivori *et al*. 2020). The Γ-peak at 15.60 Hz highlights the frequency f_4^* of the shear mode of the CB configuration (bottom of Fig. 4(b)). Significant frequency shifts of the experimental modes can be observed in the CS and CN configurations due to the presence of added masses, as synthetically reported in Table 2. It should be remarked that any other output-only identification technique can be employed to identify the experimental modes, as wells as any correlation can serve for their association with the analytical model (see Section 2.3.2).

Based on known geometric and mass properties of the frame (Table 2), the zeroth-order approximation G_{eq0} of the equivalent shear stiffness parameter G_{eq} is structurally identified through expression 21d employing the outcome of the modal identification (Table 3). The results show a good agreement among the three different configurations (consistently with the unchanged stiffness properties of the diaphragm), confirming the effectiveness of the procedure in presence of mass perturbations (previously verified analytically, see Fig. 2(a)). On the one hand, from a physical point of view, the order of magnitude of the identified equivalent shear stiffness appears smaller than the one a 100 mm concrete slab (Ponzo *et al*. 2012) is expected to provide. On the other hand, it is not straightforward to evaluate the effectiveness of the diaphragm-to-beams connections, given the presence of a HI-bond corrugated steel sheet at the interface.

The finite element model of the JetPACS frame in the CN configuration (Table 2) has been employed to further investigate the reliability of the structural identification procedure for multistory frames with asymmetric distributions of mass and stiffness. The 2S model can be regarded as the two-story extension of the one-story structure already modeled and analyzed in Section 3 (in which the in-plane constraints are released). Similarly to the previous numerical simulations, the diaphragm shear stiffness identification is carried out assuming as known the geometry and the mass properties of the frame, employing the natural frequencies provided by the finite element solution as pseudo-experimental data. The known equivalent shear stiffness parameter G_{eq} assigned to the diaphragm is increased starting from a deformable diaphragm condition, which has been manually calibrated to be representative of the experimental results (CN modal identification of Table 3). Accordingly, the rigid modes and the shear mode share neighboring frequencies of the spectrum. Increasing the shear stiffness of the diaphragm quickly moves the deformability mode to higher frequencies, leaving the rigid mode frequencies practically unchanged. The identification results, as expected, highlight a general worsening in the estimation of G_{eq} (Table 4) compared to the one-story case. The identified shear stiffness of the diaphragm is generally overestimated, but still reasonably close (same order of magnitude) to the assigned value. The simulations, finally, shed some light on the experimental identification, suggesting an overestimation – compared to the value providing a good match between the numerical frequencies and the experimental ones – of the diaphragm shear stiffness characterizing the experimental model. It should be

Table 4 Left side: values of the equivalent shear stiffness G_{eq} assigned to the rigid, semi-rigid and deformable 2S frame model and corresponding natural frequencies of the rigid (f_1^*, f_2^*, f_3^*) and shear f_4^* modes. Right side: values of the zeroth-order G_{eq0} approximation structurally identified from the pseudo-experimental frequencies

2S model	G_{eq} (N m^{-1})	f_1^* (Hz)	f_2^* (Hz)	f_3^* (Hz)	f_4^* (Hz)	G_{eq0} (N m^{-1})
Rigid	1.75×10^8	4.15	3.30	5.41	122.13	2.67×10^8
Semi-rigid	1.75×10^7	4.14	3.29	5.39	40.6	2.82×10^7
Deformable	1.75×10^6	4.07	3.22	5.30	14.1	2.98×10^6

(a) Pizzoli town hall building

(b) Concrete floor diaphragm

Fig. 5 (a) Picture of the front of the Pizzoli town hall building; (b) Detail of the floor diaphragm, highlighting the presence of iron beams drowned in the concrete slab

remarked that, however, this difference can be partially attributed to the conceptual differences between the computational and the analytical model.

4.2 Pizzoli town hall building

The Pizzoli town hall is a two-story masonry building permanently monitored by the Italian structural seismic monitoring network (synthetically referred hereinafter as OSS, Dolce *et al*. 2017). The structure rises in the Pizzoli city center (province of L'Aquila, Abruzzo, Italy) with two floors above the ground level and a non-habitable attic (Fig. 5(a)). Externally, the structure shows a certain regularity in the arrangement of the openings, which are evenly distributed along the walls and vertically aligned. The building plan has a rectangular shape of dimensions 36.75 m × 11.9 m, with the longest side oriented in the EW direction (x direction). The inter-story height increases from 3.6 m at the ground level to 4.25 m at the first level. Three main bearing walls run along the whole length of the building, evenly crossed in the front part by three secondary walls in the NS direction (y direction). The masonry piers are built with a cut local stone varying in thickness from 65 cm to 75 cm at the first level, from 30 cm to 65 cm at the second level and from 45 cm to 65 cm in the attic. A detailed structural survey – together with the documentation provided by the Italian Department of Civil Protection (made available within the context of the ReLUIS 2017-2018 Project Task 4.1, Cattari *et al*. 2019) – suggests the floor diaphragms be composed of thin iron beams and hollow bricks capped by a concrete slab, whose thickness is 16.5 cm and 12 cm at the first and the second level respectively (Fig. 5(b)).

The ambient response of the structure has been acquired by one monoaxial and three biaxial accelerometers placed at the top of each level of the building (Fig. 6(a)), with a sampling frequency of 250 Hz for one hour. The measurement setup, even if not specifically designed for

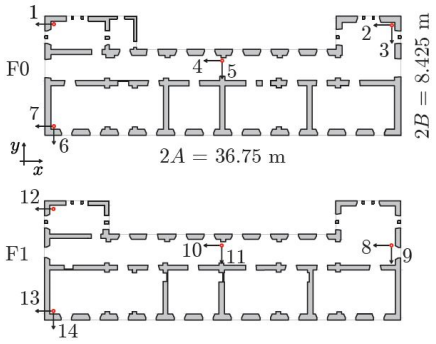

(a) Structural plans

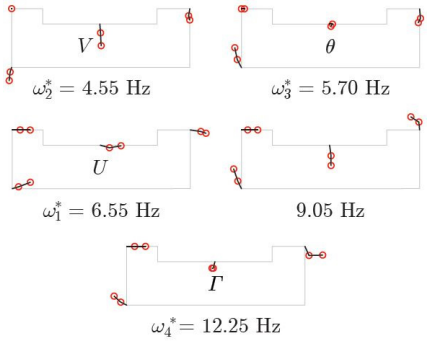

(b) Identified natural modes

Fig. 6 (a) Structural plan of the ground (F0) and first floor (F1) of the Pizzoli town hall building, highlighting the position of the sensors at the top of each level; (b) Identified natural modes

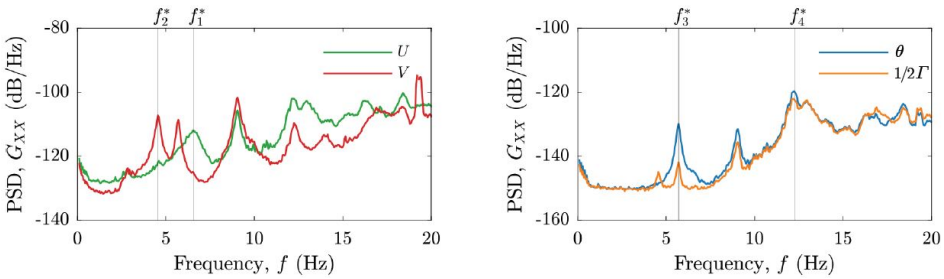

Fig. 7 (a) Power spectral densities of the rigid translations U, V and of the rigid rotation θ and shear strain Γ, estimated from the ambient response of the second floor of the Pizzoli town hall building

Table 5 Left side: natural frequencies f_1^*, f_2^*, f_3^* of the rigid modes and f_4^* of the shear mode as experimentally identified on the Pizzoli town hall building. Right side: structural identification of the zeroth-order approximation G_{eq0} of the equivalent shear stiffness from experimental frequencies

	f_1^* (Hz)	f_2^* (Hz)	f_3^* (Hz)	f_4^* (Hz)	G_{eq0} (N m^{-1})
Pizzoli	6.55	4.55	5.70	12.25	2.74×10^8

this purpose, comply with the minimum requirements to discriminate rigid diaphragm motions from shear-deformable ones (see Sivori *et al*. 2020), being present at least two biaxial sensors at the opposite vertices of each story. To this aim, natural frequencies and mode shapes are identified employing the *frequency domain decomposition* technique with a frequency resolution of 0.05 Hz (Fig. 6(b)). According to the PSD of the reconstructed rigid displacements, the rigid translation modes along the x and y directions are identified at the frequencies f_1^* and f_2^* of 6.55 Hz and 4.55 Hz respectively (left of Fig. 7). The frequency f_3^* of the torsional mode is localized at 5.70 Hz, where the contribution of θ is significantly greater than the one of the shear deformation Γ (right side of Fig. 7). The Γ-peak with the highest magnitude can be identified at 12.25 Hz (right side of Fig. 7), which is assumed as the frequency f_4^* of the shear mode (as suggested by the identified mode shape, Fig. 6(b)).

The mass of the building has been estimated assuming a masonry density of 2100 kg m^{-3} and an area density of 400 kg m^{-2} for the floor diaphragms. The perimeter walls are assumed to be evenly lumped to the diaphragm vertices, taking into account the presence of the two projecting wings. The geometric and mass parameters are thus A = 18.37 m, B = 4.21 m, $M = 1.10 \times 10^6$ kg, $m_1 = m_2 = 2.04 \times 10^5$ kg, $m_3 = m_4 = 2.04 \times 10^5 + 1.37 \times 10^5$ kg. The identified value of G_{eq} should be representative of the equivalent shear stiffness provided at the floor level by a concrete slab of average thickness 0.14 m. If we assume a concrete grade C20/25 with a Young modulus of elasticity of 3×10^{10} Pa and a Poisson ratio of 0.2, the zeroth-order approximation of the shear stiffness identified according to expression 21d (Table 5) is around one-sixth of the one which should be ideally provided by the floor slabs. From the experimental point of view, it should be remarked that several factors could influence this contribution, including but not limited to the quality of the building materials, the compliance with the execution standards, the effectiveness of the diaphragm-to-masonry connections, the possible structural aging, deterioration and damage. The last option appears the most probable explanation, since the ambient response provided by OSS has been acquired on the 1st of October 2016, after the first of the several seismic events that hit the structure in the following months (Spina *et al*. 2019). Nevertheless, as it will be proposed in the following, the structural identification procedure can be useful to improve the calibration of more detailed computational models.

To this aim, an equivalent-frame (EF) model of the building has been employed (Fig. 8(a)) by using the software Tremuri (Lagomarsino *et al*. 2013). Accordingly, the resistant masonry walls are described with deformable masonry panels (piers and spandrels, respectively in orange and green in Fig. 8(a)) in which the deformation and the nonlinear response are concentrated, connected to each other from rigid portions (rigid nodes, cyan in Fig. 8(a)). The vertical resistant elements, whose contribution is related to their in-plane strength and stiffness, are assembled through orthotropic membranes (plane stress regime) representing the floor diaphragms. Thanks to the low number of degrees of freedom, this approach has limited computational requirements and, thus, it is commonly employed in the nonlinear seismic analyses of masonry buildings. The building model is based on the geometrical and structural characteristics obtained from the in-situ survey and the available graphical documentation (Cattari *et al*. 2019). For what concerns the mechanical properties of the masonry, in accordance with the values suggested by the Italian National Building Code for this typology (see the Italian Circular 21/1/19 No. 7), the Young elastic modulus is assumed to be equal to 2.7×10^9 Pa for the free undamped dynamics of the model to be representative of experimental data (left side of Table 5). This is also compatible with reference values proposed in the literature, derived from experimental data on similar masonry typologies (Kržan *et al*. 2015, Vanin *et al*. 2017).

The solution of the eigenvalue problem provided by the EF model following the diaphragm stiffness calibration –

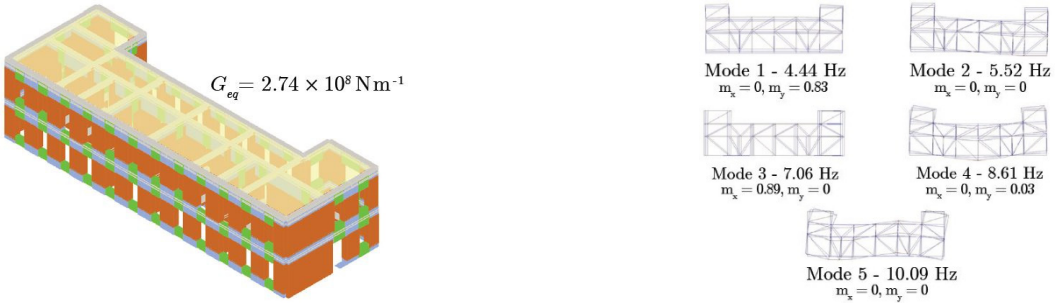

(a) Equivalent-frame model (b) Natural modes

Fig. 8 (a) Equivalent frame (EF) model of the Pizzoli town hall building; (b) First five natural frequencies and mode shapes assuming the equivalent shear stiffness of the diaphragm structurally identified

Table 6 Natural frequencies of the EF model of Pizzoli town hall building, varying the equivalent shear stiffness of the diaphragm starting from the identified value. Relative difference in frequency δf and MAC matrix between the numerical and the experimental mode shapes

	$G_{eq} = 9.1 \times 10^7$ N m^{-1}					$G_{eq} = 2.74 \times 10^8$ N m^{-1}					$G_{eq} = 8.22 \times 10^8$ N m^{-1}				
f (Hz)	4.08	4.77	6.61	6.76	7.56	4.44	5.52	7.06	8.61	10.09	4.55	5.75	7.07	10.39	11.54
δf	0.10	0.16	-0.01	0.25	0.38	0.02	0.03	-0.08	0.05	0.18	0	-0.01	-0.08	-0.15	0.06
4.55	0.95	0	0.01	0	0	0.97	0	0	0.01	0	0.96	0.01	0.	0.02	0
5.70	0.02	0.89	0	0.02	0.60	0.03	0.94	0.01	0.02	0.43	0.04	0.91	0.01	0.01	0
6.55	0	0.02	0	0.95	0.22	0.01	0.08	0.95	0	0.28	0.01	0.11	0.95	0	0
9.05	0.01	0.01	0.77	0.01	0.15	0	0.02	0	0.93	0.03	0.02	0.02	0	0.86	0.17
12.25	0.03	0.15	0.01	0.14	0.70	0.01	0.35	0.08	0.05	0.76	0.01	0.42	0.07	0.04	0

assuming the identified zeroth-order value G_{eq0} reported in Table 5 as the equivalent shear stiffness of the floor membranes – highlights a good correlation between the numerical and the experimental mode shapes (center of Table 6). In particular, also the fourth and fifth experimentally identified modes, which involve respectively the in-plane bending and shear deformation of the floor diaphragms (Fig. 6(b)), are correctly reproduced by the model (Fig. 8(b)), as highlighted by the high values of the modal assurance criterion (MAC, Allemang 2003) computed with respect to the experimental mode shapes. It should be noted, moreover, how the mode shapes appear to be quite sensitive to variations of the diaphragm shear stiffness, as shown by the sudden decrease in the MAC values for both more deformable and more stiff diaphragms (respectively one third and three times the identified shear stiffness, left and right side of Table 6). On the other hand, the discrepancy between the numerical and the experimental frequency of the shear deformability mode could be attributed to the mass distribution of the EF frame which, at the floor level, is lumped to the perimeter nodes, increasing the floor rotational inertia. The reliability of the EF model of the Pizzoli town hall building has been further discussed in Cattari *et al*. (2019) and in Degli Abbati *et al*. (2021), referring to the good accordance between the simulated seismic response and the acceleration recordings acquired on the structure during the 2016/2017 Central Italy earthquake sequence.

It is observed that, in this specific case, the calibration of the shear stiffness of the floor diaphragms affects particularly the frequencies and mode shapes of the high-frequency natural modes (fourth and fifth modes). Although associated with a modest participating mass (Fig. 8(b)) and, thus, to a minor influence on the seismic response of the structure, these modes can still be significant in the correct evaluation of local effects, such as the estimation of local deformations at the floor level. This indicator can be employed to estimate the expected damage and the related economic losses, as studied in recent developments of seismic engineering (Del Vecchio *et al*. 2018, 2020, Ottonelli *et al*. 2020, Cardone *et al*. 2020) and motivated by the heavy social impacts highlighted by Italian seismic events (Di Ludovico *et al*. 2017a, b).

5. Conclusions

The mechanical assumption of in-plane rigidity or deformability of the floor diaphragms is a fundamental issue in the formulation of analytical and computational models of buildings. Therefore, the development of reliable procedures to quantitatively assess the diaphragm stiffness of existing buildings is a topical matter of theoretical and practical interest. Unreinforced masonry buildings, in particular, may present a large variability range in the assessment of the diaphragm stiffness, due to a number of technical and constructional configurations.

Based on these motivations, a model-based technique has been proposed to analytically determine the diaphragm stiffness in existing buildings, by leveraging the increasing

availability of spectral information from operational modal analyses (first-level modal identification problem). Starting from this knowledge, the inverse problem of parametrically identifying the diaphragm in-plane shear stiffness (second-level parametric or structural identification problem) has been attacked.

First, a low-dimension discrete model of the diaphragm has been formulated to describe the linear undamped dynamics of the building floor. The shear deformability of the diaphragm has been taken into account by adding an extra dynamically-active degree-of-freedom. The structural matrices of the model have been built analytically. Afterward, the direct eigenproblem governing the modal properties has been stated and solved. The complete eigen-solution has been obtained in a suited analytic – although asymptotically approximate – fashion (direct problem solution). To this purpose, a general asymptotic strategy to achieve analytical approximations of the frequencies and modes has been outlined, under the assumption of no internal resonances. The strategy allows to analytically determine the modal quantities as explicit functions of the mechanical parameters for dynamic model of generic dimensions, up to the desired order of approximation. The local validity of the frequency approximations has been discussed, and its accuracy has been satisfyingly verified by numerical sensitivity analyses under small perturbations of the mass and stiffness matrices.

Second, the low-order approximations have been considered in order to state analytically invertible spectral relations between the mechanical parameters and the modal quantities. Assuming experimentally known part of the modal quantities – from operational modal analyses – the inversion of the spectral relations has made possible the identification of the mechanical parameters (inverse problem solution). Specifically, explicit formulas have been determined to assess the principal stiffness parameters, including the shear stiffness of the diaphragm, as explicit functions of the experimental frequencies. Consistently with the asymptotic nature of the inverse problem solution, a minimal uncoupled structural model has been identified considering the lowest order of the inverse solution (model identification). Therefore, a refined coupled structural model, including mass and stiffness eccentricities, has been identified considering higher orders of the inverse solution (model updating).

Third, the accuracy of the structural identification has been numerically verified through pseudo-experimental data, generated from the finite element model of a simple frame structure. Finally, the effectiveness of the procedure has been successfully tested experimentally, by employing dynamic measurements from laboratory tests on scaled models, as well as vibration recordings from the full-scale monitoring of an existing masonry building. Results on the latter are quite promising from an engineering point of view, highlighting the potential of the procedure in the use of ambient vibration tests to support, guide or validate the modeling choices, as well as to reduce the uncertainties intrinsic to the knowledge of existing buildings.

Acknowledgments

The results presented in this paper are obtained with the partial funding of the ReLUIS Project 2019–2021 (Work Package 6). Moreover, the validation carried out on the Pizzoli town hall benefited of the data made available by the Italian structural seismic monitoring network (OSS) of the Italian Department of Civil Protection, within the research activities of ReLUIS Project 2017-2018 (WP4 Task 4.1).

References

Allemang, R.J. (2003), "The modal assurance criterion – Twenty years of use and abuse", *Sound Vib*., **37**(8), 1423.

ASCE 41-13 (2014), "Seismic Evaluation and Retrofit of Existing Buildings", Reston, VA, USA.

Astorga, A., Guéguen, P., Ghimire, S. and Kashima, T. (2020), "NDE1. 0: a new database of earthquake data recordings from buildings for engineering applications", *Bull. Earthq. Eng.*, **18**(4), 1321-1344. https://doi.org/10.1007/s10518-019-00746-6

Boschi, S., Galano, L. and Vignoli, A. (2019), "Mechanical characterisation of Tuscany masonry typologies by in situ tests", *Bull. Earthq. Eng*., **17**(1), 413-438. https://doi.org/10.1007/s10518-018-0451-4

Bracchi, S., Rota, M., Penna, A. and Magenes, G. (2015), "Consideration of modelling uncertainties in the seismic assessment of masonry buildings by equivalent-frame approach", *Bull. Earthq. Eng*., **13**(11), 3423-3448. https://doi.org/10.1007/s10518-015-9760-z

Brincker, R., Zhang, L. and Andersen, P. (2001), "Modal identification of output-only systems using frequency domain decomposition", *Smart Mater. Struct*., **10**(3), 441. https://doi.org/doi:10.1088/0964-1726/10/3/303

Cardone, D., Perrone, G. and Flora, A. (2020), "Displacement-Based Simplified Seismic Loss Assessment of Pre70S RC Buildings", *J. Earthq. Eng*., **24**(sup1), 82-113. https://doi.org/10.1080/13632469.2020.1716890

Cattari, S., Resemini, S. and Lagomarsino, S. (2008), "Modelling of vaults as equivalent diaphragms in 3D seismic analysis of masonry buildings", In: *Structural Analysis of Historic Construction*: *Preserving Safety and Significance*, Two Volume Set (pp. 537-544), CRC Press.

Cattari, S., Lagomarsino, S., Karatzetzou, A. and Pitilakis, D. (2015), "Vulnerability assessment of Hassan Bey's mansion in Rhodes", *Bull. Earthq. Eng*., **13**(1), 347-368. https://doi.org/10.1007/s10518-014-9613-1

Cattari, S., Degli Abbati, S., Ottonelli, D., Marano, C., Camata, G., Spacone, E., Da Porto, F., Modena, C., Lorenzoni, F., Magenes, G. and Penna, A. (2019), "Discussion on data recorded by the Italian structural seismic monitoring network on three masonry structures hit by the 2016-2017 Central Italy earthquake", *Proceedings of the 7th International Conference on Computational Methods in Structural Dynamics and Earthquake Engineering* (*COMPDYN2019*), Crete, Greece. https://doi.org/10.7712/120119.7044.20004

Circular 21/1/19 No. 7 (2019), "Istruzioni per l'applicazione dell'aggiornamento delle norme tecniche per le costruzioni di cui al Decreto Ministeriale 17 Gennaio 2018", Ministry of Infrastructures and Transportation, Rome, Italy. [In Italian]

Degli Abbati, S., Morandi, P., Spacone, E. (2021), "On the reliability of the equivalent frame models: the case study of the permanently monitored Pizzoli's town hall", *Bull. Earthq. Eng.* [Submitted]

Del Gaudio, C., De Martino, G., Di Ludovico, M., Manfredi, G.,

Prota, A., Ricci, P. and Verderame, G.M. (2019), "Empirical fragility curves for masonry buildings after the 2009 L'Aquila, Italy, earthquake", *Bull. Earthq. Eng.*, **17**(11), 6301-6330. https://doi.org/10.1007/s10518-019-00683-4

Del Vecchio, C., Di Ludovico, M., Pampanin, S. and Prota, A. (2018), "Repair costs of existing RC buildings damaged by the L'Aquila earthquake and comparison with FEMA P58 predictions", *Earthq. Spectra*, **34**(1), 237-263. https://doi.org/10.1193/122916EQS257M

Del Vecchio, C., Di Ludovico, M. and Prota, A. (2020), "Repair costs of reinforced concrete building components: from actual data analysis to calibrated consequence functions", *Earthq. Spectra*, **36**(1), 353-377. https://doi.org/10.1193/122916EQS257M

Derkevorkian, A., Masri, S.F., Fujino, Y. and Siringoringo, D.M. (2014), "Development and validation of nonlinear computational models of dispersed structures under strong earthquake excitation", *Earthq. Eng. Struct. Dyn.*, **43**(7), 1089-1105. https://doi.org/10.1002/eqe.2389

Di Ludovico, M., Prota, A., Moroni, C., Manfredi, G. and Dolce, M. (2017a), "Reconstruction process of damaged residential buildings outside historical centres after the L'Aquila earthquake: part I—"light damage" reconstruction", *Bull. Earthq. Eng.*, **15**(2), 667-692. https://doi.org/10.1007/s10518-016-9877-8

Di Ludovico, M., Prota, A., Moroni, C., Manfredi, G. and Dolce, M. (2017b), "Reconstruction process of damaged residential buildings outside historical centres after the L'Aquila earthquake: part II—"heavy damage" reconstruction", *Bull. Earthq. Eng.*, **15**(2), 693-729. https://doi.org/10.1007/s10518-016-9979-3

Dizhur, D., Wei, S., Giaretton, M., Schultz, A.E., Ingham, J.M. and Giongo, I. (2020), "Testing of URM wall-to-diaphragm through-bolt plate anchor connections", *Earthq. Spectra*, 8755293020944187. https://doi.org/10.1177/8755293020944187

Dolce, M., Ponzo, F.C., Di Cesare, A., Ditommaso, R., Moroni, C., Nigro, D., Serino, G., Sorace, S., Gattulli, V., Occhiuzzi, A., Vulcano, A., Foti, D. (2008), "Jetpacs project: joint experimental testing on passive and semiactive control systems", *Proceedings of the 14th World Conference on Earthquake Engineering* (*14WCEE*), Beijing, China. https://doi.org/10.1080/13632469.2012.657335

Dolce, M., Nicoletti, M., De Sortis, A., Marchesini, S., Spina, D. and Talanas, F. (2017), "Osservatorio sismico delle strutture: the Italian structural seismic monitoring network", *Bull. Earthq. Eng.*, **15**(2), 621-641. https://doi.org/10.1007/s10518-015-9738-x.

Dolce, M., Speranza, E., Giordano, F., Borzi, B., Bocchi, F., Conte, C., Di Meo, A., Faravelli, M. and Pascale, V. (2019), "Observed damage database of past Italian earthquakes: the Da.D.O WebGIS", *Bollettino di Geofisica Teorica ed Applicata*, **60**(2). https://doi.org/10.4430/bgta0254

EN19983 (2005), "Eurocode 8: Design of structures for earthquake resistance Part 3: Assessment and retrofitting of buildings".

Gattulli, V., Lepidi, M. and Potenza, F. (2009), "Seismic protection of frame structures via semiactive control: modeling and implementation issues", *Earthq. Eng. Eng. Vib.*, **8**(4), 627-645. https://doi.org/10.1007/s11803-009-9113-5

Gattulli, V., Lepidi, M. and Potenza, F. (2016), "Dynamic testing and health monitoring of historic and modern civil structures in Italy", *Struct. Monitor. Maint., Int. J.*, **3**(1), 71-90. https://doi.org/10.12989/smm.2016.3.1.071

Giongo, I., Dizhur, D., Tomasi, R. and Ingham, J.M. (2015), "Field testing of flexible timber diaphragms in an existing vintage URM building", *J. Struct. Eng.*, **141**(1), D4014009. https://doi.org/10.1061/(ASCE)ST.1943-541X.0001045

Greco, A., Fiore, I., Occhipinti, G., Caddemi, S., Spina, D. and Caliò, I. (2020), "An Equivalent Non-Uniform Beam-Like Model for Dynamic Analysis of Multi-Storey Irregular Buildings", *Appl. Sci.*, **10**(9), 3212. https://doi.org/10.3390/app10093212

Haddad, J., Cattari, S. and Lagomarsino, S. (2019), "Use of the model parameter sensitivity analysis for the probabilistic-based seismic assessment of existing buildings", *Bull. Earthq. Eng.*, **17**(4), 1983-2009. https://doi.org/10.1007/s10518-018-0520-8

Hajj, M.R., Fung, J., Nayfeh, A.H. and Fahey, S.F. (2000), "Damping identification using perturbation techniques and higher-order spectra", *Nonlinear Dyn.*, **23**(2), 189-203. https://doi.org/10.1023/A:1008335522973

Iervolino, I., Giorgio, M. and Chioccarelli, E. (2014), "Closed-form aftershock reliability of damage-cumulating elastic-perfectly-plastic systems", *Earthq. Eng. Struct. Dyn.*, **43**(4), 613-625. https://doi.org/10.1002/eqe.2363

Jaishi, B. and Ren, W.X. (2005), "Structural finite element model updating using ambient vibration test results", *J. Struct. Eng.*, **131**(4), 617-628. https://doi.org/10.1061/(ASCE)0733-9445(2005)131:4(617)

Jalayer, F., Iervolino, I. and Manfredi, G. (2010), "Structural modeling uncertainties and their influence on seismic assessment of existing RC structures", *Struct. Safety*, **32**(3), 220-228. https://doi.org/10.1016/j.strusafe.2010.02.004

Karatzetzou, A., Negulescu, C., Manakou, M., François, B., Seyedi, D.M., Pitilakis, D. and Pitilakis, K. (2015), "Ambient vibration measurements on monuments in the Medieval City of Rhodes, Greece", *Bull. Earthq. Eng.*, **13**(1), 331-345. https://doi.org/10.1007/s10518-014-9649-2

Kerschen, G., Worden, K., Vakakis, A.F. and Golinval, J.C. (2006), "Past, present and future of nonlinear system identification in structural dynamics", *Mech. Syst. Signal Process.*, **20**(3), 505-592. https://doi.org/10.1016/j.ymssp.2005.04.008

Kosič, M., Fajfar, P. and Dolšek, M. (2014), "Approximate seismic risk assessment of building structures with explicit consideration of uncertainties", *Earthq. Eng. Struct. Dyn.*, **43**(10), 1483-1502. https://doi.org/10.1002/eqe.2407

Kržan, M., Gostič, S., Cattari, S. and Bosiljkov, V. (2015), "Acquiring reference parameters of masonry for the structural performance analysis of historical buildings", *Bull. Earthq. Eng.*, **13**(1), 203-236. https://doi.org/10.1007/s10518-014-9686-x

Kunnath, S.K., Panahshahi, N. and Reinhorn, A.M. (1991), "Seismic response of RC buildings with inelastic floor diaphragms", *J. Struct. Eng.*, **117**(4), 1218-1237. https://doi.org/10.1061/(ASCE)07339445(1991)117:4(1218)

Lacarbonara, W., Carboni, B. and Quaranta, G. (2016), "Nonlinear normal modes for damage detection", *Meccanica*, **51**(11), 2629-2645. https://doi.org/10.1007/s11012-016-0453-8

Lagomarsino, S. and Giovinazzi, S. (2006), "Macroseismic and mechanical models for the vulnerability and damage assessment of current buildings", *Bull. Earthq. Eng.*, **4**(4), 415-443. https://doi.org/10.1007/s105180069024z

Lagomarsino, S., Penna, A., Galasco, A. and Cattari, S. (2013), "TREMURI program: an equivalent frame model for the nonlinear seismic analysis of masonry buildings", *Eng. Struct.*, **56**, 1787-1799. https://doi.org/10.1016/j.engstruct.2013.08.002

Lee, Y.S., Vakakis, A.F., McFarland, D.M. and Bergman, L.A. (2010), "A global–local approach to nonlinear system identification: a review", *Struct. Control Health Monitor.*, **17**(7), 742-760. https://doi.org/10.1002/stc.414

Lepidi, M. (2013), "Multi-parameter perturbation methods for the eigensolution sensitivity analysis of nearly-resonant non-defective multi-degree-of-freedom systems", *J. Sound Vib.*, **332**(4), 1011-1032. https://doi.org/10.1016/j.jsv.2012.09.020

Lepidi, M. and Bacigalupo, A. (2018), "Multi-parametric

sensitivity analysis of the band structure for tetrachiral acoustic metamaterials", *Int. J. Solids Struct.*, **136**, 186-202. https://doi.org/10.1016/j.ijsolstr.2017.12.014

Lepidi, M. and Gattulli, V. (2014), "A parametric multibody section model for modal interactions of cable-supported bridges", *J. Sound Vib.*, **333**(19), 4579-4596. https://doi.org/10.1016/j.jsv.2014.04.053

Lofrano, E., Paolone, A. and Vasta, M. (2016), "A perturbation approach for the identification of uncertain structures", *Int. J. Dyn. Control*, **4**(2), 204-212. https://doi.org/10.1007/s40435-015-0171-4

Luongo, A. (2017), "On the use of the multiple scale method in solving 'difficult' bifurcation problems", *Mathe. Mech. Solids*, **22**(5), 988-1004. https://doi.org/10.1177/1081286515616053

Lupoi, G., Calvi, G.M., Lupoi, A. and Pinto, P.E. (2004), "Comparison of different approaches for seismic assessment of existing buildings", *J. Earthq. Eng.*, **8**(1), 121-160. https://doi.org/10.1080/13632460409350523

Marino, S., Cattari, S. and Lagomarsino, S. (2019), "Are the nonlinear static procedures feasible for the seismic assessment of irregular existing masonry buildings?", *Eng. Struct.*, **200**, 109700. https://doi.org/10.1016/j.engstruct.2019.109700

Michel, C., Gueguen, P. and Causse, M. (2012), "Seismic vulnerability assessment to slight damage based on experimental modal parameters", *Earthq. Eng. Struct. Dyn.*, **41**(1), 81-98. https://doi.org/10.1002/eqe.1119

Mori, F. and Spina, D. (2015), "Vulnerability assessment of strategic buildings based on ambient vibrations measurements", *Struct. Monitor. Maint., Int. J.*, **2**(2), 115-132. https://doi.org/10.12989/smm.2015.2.2.115

Mottershead, J.E., Link, M. and Friswell, M.I. (2011), "The sensitivity method in finite element model updating: A tutorial", *Mech. Syst. Signal Process.*, **25**(7), 2275-2296. https://doi.org/10.1016/j.ymssp.2010.10.012

Nakamura, Y., Derakhshan, H., Magenes, G. and Griffith, M.C. (2017), "Influence of diaphragm flexibility on seismic response of unreinforced masonry buildings", *J. Earthq. Eng.*, **21**(6), 935-960. https://doi.org/10.1080/13632469.2016.1190799

NTC (2018), "The Italian Building Code", Ministry of Infrastructures and Transportation, Rome, Italy. [In Italian]

NZSEE (2017), "The Seismic Assessment of Existing Buildings", Wellington, New Zealand.

Ottonelli, D., Cattari, S. and Lagomarsino, S. (2020), "Displacement-Based Simplified Seismic Loss Assessment of Masonry Buildings", *J. Earthq. Eng.*, **24**(sup1), 23-59. https://doi.org/10.1080/13632469.2020.1755747

Ponzo, F.C., Di Cesare, A., Nigro, D., Vulcano, A., Mazza, F., Dolce, M. and Moroni, C. (2012), "JETPACS project: dynamic experimental tests and numerical results obtained for a steel frame equipped with hysteretic damped chevron braces", *J. Earthq. Eng.*, **16**(5), 662-685. https://doi.org/10.1080/13632469.2012.657335

Reynders, E., Teughels, A. and De Roeck, G. (2010), "Finite element model updating and structural damage identification using OMAX data", *Mech. Syst. Signal Process.*, **24**(5), 1306-1323. https://doi.org/10.1016/j.ymssp.2010.03.014

Rizzi, E., Giongo, I., Ingham, J.M. and Dizhur, D. (2020), "Testing and Modeling In-Plane Behavior of Retrofitted Timber Diaphragms", *J. Struct. Eng.*, **146**(2), 04019191. https://doi.org/10.1061/(ASCE)ST.1943541X.0002473

Rossi, M., Calderini, C. and Lagomarsino, S. (2016), "Experimental testing of the seismic in-plane displacement capacity of masonry cross vaults through a scale model", *Bull. Earthq. Eng.*, **14**(1), 261-281. https://doi.org/10.1007/s10518-015-9815-1

Rossi, M., Barentin, C.C., Van Mele, T. and Block, P. (2017), "Experimental study on the behaviour of masonry pavilion vaults on spreading supports", In: *Structures* (Vol. 11, pp. 110120), Elsevier. https://doi.org/10.1016/j.istruc.2017.04.008

Rosti, A., Rota, M. and Penna, A. (2020), "Empirical fragility curves for Italian URM buildings", *Bull. Earthq. Eng.* https://doi.org/10.1007/s10518-015-9815-1

Sivori, D., Lepidi, M. and Cattari, S. (2020), "Ambient vibration tools to validate the rigid diaphragm assumption in the seismic assessment of buildings", *Earthq. Eng. Struct. Dyn.*, **49**(2), 194-211. https://doi.org/10.1002/eqe.3235

Solarino, F., Oliveira, D.V. and Giresini, L. (2019), "Wall-to-horizontal diaphragm connections in historical buildings: A state-of-the-art review", *Eng. Struct.*, **199**, 109559. https://doi.org/10.1016/j.engstruct.2019.109559

Spina, D., Acunzo, G., Fiorini, N., Mori, F. and Dolce, M. (2019), "A probabilistic simplified seismic model of masonry buildings based on ambient vibrations", *Bull. Earthq. Eng.*, **17**(2), 985-1007. https://doi.org/10.1007/s10518-018-0481-y

Vanin, F., Zaganelli, D., Penna, A. and Beyer, K. (2017), "Estimates for the stiffness, strength and drift capacity of stone masonry walls based on 123 quasistatic cyclic tests reported in the literature", *Bull. Earthq. Eng.*, **15**(12), 5435-5479. https://doi.org/10.1007/s10518-017-0188-5

Zárate, B.A. and Caicedo, J.M. (2008), "Finite element model updating: Multiple alternatives", *Eng. Struct.*, **30**(12), 3724-3730. https://doi.org/10.1016/j.engstruct.2008.06.012

A. Appendices

A.1 Governing matrices

With reference to the twelve-by-one displacement vector $\mathbf{u} = (u_1,\ v_1,\ u_2,\ v_2,\ u_3,\ v_3,\ u_4,\ v_4,\ u,\ v,\ \theta,\ \Gamma)$ of the unconstrained model, the twelve-by-twelve mass and stiffness matrices read

$$\mathbf{M} = \begin{bmatrix} \mathbf{M}_{11} & \mathbf{M}_{12} & \mathbf{M}_{13} \\ \mathbf{M}_{21} & \mathbf{M}_{22} & \mathbf{M}_{23} \\ \mathbf{M}_{31} & \mathbf{M}_{32} & \mathbf{M}_{33} \end{bmatrix}, \qquad \mathbf{K} = \begin{bmatrix} \mathbf{K}_{11} & \mathbf{K}_{12} & \mathbf{K}_{13} \\ \mathbf{K}_{21} & \mathbf{K}_{22} & \mathbf{K}_{23} \\ \mathbf{K}_{31} & \mathbf{K}_{32} & \mathbf{K}_{33} \end{bmatrix}$$

where the not-null mass submatrices are

$$\mathbf{M}_{11} = \begin{bmatrix} \varrho_1^2 & 0 & 0 & 0 \\ 0 & \varrho_1^2 & 0 & 0 \\ 0 & 0 & \varrho_2^2 & 0 \\ 0 & 0 & 0 & \varrho_2^2 \end{bmatrix},$$

$$\mathbf{M}_{22} = \begin{bmatrix} \varrho_3^2 & 0 & 0 & 0 \\ 0 & \varrho_3^2 & 0 & 0 \\ 0 & 0 & \varrho_4^2 & 0 \\ 0 & 0 & 0 & \varrho_4^2 \end{bmatrix},$$

$$\mathbf{M}_{33} = \begin{bmatrix} 1 & 0 & 0 & 0 \\ 0 & 1 & 0 & 0 \\ 0 & 0 & \chi^2 & 0 \\ 0 & 0 & 0 & \frac{1}{4}\beta^2\chi^2 \end{bmatrix}$$

In particular, the term $\frac{1}{4}\beta^2\chi^2$ relates the shear deformation inertia to the rotational inertia χ^2 trough the expression

$$J_\Gamma = \frac{1}{3}\frac{B^2}{A^2}M(A^2+B^2) = \frac{1}{4}\frac{B^2}{A^2}J$$

where M is the translational mass. The not-null stiffness submatrices are

$$\mathbf{K}_{11} = \begin{bmatrix} \frac{\kappa_s}{\beta^2+1} + \kappa_{x1} & \frac{\beta\kappa_s}{\beta^2+1} & 0 & 0 \\ \frac{\beta\kappa_s}{\beta^2+1} & \frac{\beta^2\kappa_s}{\beta^2+1} + \kappa_{y1} & 0 & 0 \\ 0 & 0 & \frac{\kappa_s}{\beta^2+1} + \kappa_{x2} & -\frac{\beta\kappa_s}{\beta^2+1} \\ 0 & 0 & -\frac{\beta\kappa_s}{\beta^2+1} & \frac{\beta^2\kappa_s}{\beta^2+1} + \kappa_{y2} \end{bmatrix},$$

$$\mathbf{K}_{12} = \begin{bmatrix} -\frac{\kappa_s}{\beta^2+1} & -\frac{\beta\kappa_s}{\beta^2+1} & 0 & 0 \\ -\frac{\beta\kappa_s}{\beta^2+1} & -\frac{\beta^2\kappa_s}{\beta^2+1} & 0 & 0 \\ 0 & 0 & -\frac{\kappa_s}{\beta^2+1} & \frac{\beta\kappa_s}{\beta^2+1} \\ 0 & 0 & \frac{\beta\kappa_s}{\beta^2+1} & -\frac{\beta^2\kappa_s}{\beta^2+1} \end{bmatrix}$$

$$\mathbf{K}_{22} = \begin{bmatrix} \frac{\kappa_s}{\beta^2+1} + \kappa_{x3} & \frac{\beta\kappa_s}{\beta^2+1} & 0 & 0 \\ \frac{\beta\kappa_s}{\beta^2+1} & \frac{\beta^2\kappa_s}{\beta^2+1} + \kappa_{y3} & 0 & 0 \\ 0 & 0 & \frac{\kappa_s}{\beta^2+1} + \kappa_{x4} & -\frac{\beta\kappa_s}{\beta^2+1} \\ 0 & 0 & -\frac{\beta\kappa_s}{\beta^2+1} & \frac{\beta^2\kappa_s}{\beta^2+1} + \kappa_{y4} \end{bmatrix}$$

and, for the sake of symmetry, $\mathbf{K}_{21} = \mathbf{K}_{12}$.

The rectangular constraint matrices $\mathbf{V}_r$ and $\mathbf{V}_d$ of the rigid model, characterized by the three-by-one vector $\mathbf{q}_r = (u, v, \theta)$ of free degrees-of-freedom, and of the deformable model, characterized instead by the four-by-one free vector $\mathbf{q}_d = (u, v, \theta, \Gamma)$ of free degrees-of-freedom, are

$$\mathbf{V}_r = \begin{bmatrix} 1 & 0 & -\beta \\ 0 & 1 & 1 \\ 1 & 0 & -\beta \\ 0 & 1 & -1 \\ 1 & 0 & \beta \\ 0 & 1 & -1 \\ 1 & 0 & \beta \\ 0 & 1 & 1 \\ 0 & 0 & 0 \end{bmatrix}, \qquad \mathbf{V}_d = \begin{bmatrix} 1 & 0 & -\beta & \frac{1}{2}\beta \\ 0 & 1 & 1 & \frac{1}{2}\beta^2 \\ 1 & 0 & -\beta & \frac{1}{2}\beta \\ 0 & 1 & -1 & -\frac{1}{2}\beta^2 \\ 1 & 0 & \beta & -\frac{1}{2}\beta \\ 0 & 1 & -1 & -\frac{1}{2}\beta^2 \\ 1 & 0 & \beta & -\frac{1}{2}\beta \\ 0 & 1 & 1 & \frac{1}{2}\beta^2 \end{bmatrix}$$

A.2 Perturbation matrices

The perturbation mass and stiffness matrices introduced in Section 2.3.1 are

$$\mathbf{M}_d^\circ = \begin{bmatrix} 1+\Sigma_\varrho^2 & 0 & 0 & 0 \\ 0 & 1+\Sigma_\varrho^2 & 0 & 0 \\ 0 & 0 & \chi_0^2+\Sigma_\theta^2 & 0 \\ 0 & 0 & 0 & \frac{1}{4}\beta^2(\chi_0^2+\Sigma_\theta^2) \end{bmatrix},$$

$$\mathbf{K}_d^\circ = \begin{bmatrix} \Sigma_{\kappa x} & 0 & 0 & 0 \\ 0 & \Sigma_{\kappa y} & 0 & 0 \\ 0 & 0 & \Sigma_{\kappa\theta} & 0 \\ 0 & 0 & 0 & \beta_\Gamma\kappa_{S0} + \Sigma_{\kappa\Gamma} \end{bmatrix},$$

$$\boldsymbol{M}_d' = \begin{bmatrix} 0 & 0 & -2\beta\Delta_{\varrho x1}^2 & \beta\Delta_{\varrho x1}^2 \\ 0 & 0 & 2\Delta_{\varrho y1}^2 & \beta^2\Delta_{\varrho y1}^2 \\ -2\beta\Delta_{\varrho x1}^2 & 2\Delta_{\varrho y1}^2 & \beta^2\Delta_{\varrho y1}^2 & 0 \\ \beta\Delta_{\varrho x1}^2 & \beta^2\Delta_{\varrho y1}^2 & 0 & \frac{1}{4}\beta^2\chi_1^2 \end{bmatrix},$$

$$\mathbf{K}_d' = \begin{bmatrix} 0 & 0 & -2\beta\Delta_{\kappa x1} & \beta\Delta_{\kappa x1} \\ 0 & 0 & 2\Delta_{\kappa y1} & \beta^2\Delta_{\kappa y1} \\ -2\beta\Delta_{\kappa x1} & 2\Delta_{\kappa y1} & 0 & -\beta^2\Delta_{\kappa xy1} \\ \beta\Delta_{\kappa x1} & \beta^2\Delta_{\kappa y1} & -\beta^2\Delta_{\kappa xy1} & \beta_\Gamma\kappa_{S1} \end{bmatrix}$$